LA-11065

High-Strain-Rate, High-Temperature Biaxial Testing of DOP-26 Iridium

Los Alamos

Los Alamos National Laboratory is operated by the University of California for the United States Department of Energy under contract W-7405-ENG-36.

DISCLAIMER

Edited by Renate Lewin
Photocomposition by Debi Erpenbeck

This work was supported by the US Department of Energy, Office of Special Nuclear Projects.

An Affirmative Action/Equal Opportunity Employer

LA-11065

UC-~~25~~ 704
Issued: May 1988

LA--11065

DE88 010471

High-Strain-Rate, High-Temperature Biaxial Testing of DOP-26 Iridium

T. G. George

Los Alamos National Laboratory
Los Alamos, New Mexico 87545

HIGH-STRAIN-RATE, HIGH-TEMPERATURE BIAXIAL TESTING OF DOP-26 IRIDIUM

by

T. G. George

ABSTRACT

High-strain-rate biaxial punch tests were performed on DOP-26 (Ir-0.3 wt% tungsten) iridium-alloy discs given annealing and aging heat treatments. Test temperatures ranged between 600°C and 1440°C, and punch velocity was held constant at 45 m/s. Three types of samples were evaluated: Z-batch old-process discs, B-batch old-process discs, and B-batch new-process discs. The results indicate that batch-to-batch variations in ductility are significant and that new-process iridium is slightly more ductile than old-process material.

I. INTRODUCTION

DOP-26 iridium alloy (iridium-0.3 wt% tungsten) is used to encapsulate the $^{238}PuO_2$ fuel in radioisotope thermoelectric generators that provide electric power for interplanetary spacecraft. Because the iridium alloy is the primary containment vessel for the plutonia fuel, a great deal of effort has been expended trying to evaluate and predict conditions under which the cladding might breach. Tests conducted at the Los Alamos National Laboratory, in which fueled capsules were subjected to simulated reentry and earth-impact conditions,[1–5] demonstrated that the loads generated during impact could cause clad failure. Postmortem examination of the capsules used in these tests also revealed clear evidence of strain-state sensitivity in the iridium alloy. These findings prompted the initiation of a high-strain-rate biaxial test program, to produce a forming limit diagram for DOP-26 iridium that would predict its behavior at high strain rates.

The concept of a forming limit diagram was developed by Keeler[6] and Goodwin[7] from their work with steel stampings. Subsequent researchers, such as Ghosh[8] and Hecker,[9] successfully utilized forming limit diagrams to describe the deformation of other materials. In essence, a forming limit diagram depicts the effect of loading condition on a material's deformation stability (strain to failure). A typical forming limit diagram may be seen in Fig. 1. As the diagram shows, minor engineering strains are plotted along the X axis, and major engineering strain is plotted along the Y axis. The region to the left of the Y axis represents variations of uniaxial (simple) tension, and the region to the right of the Y axis represents variants of biaxial tension (stretching). Points along the Y axis (minor strain = 0) represent a loading condition analogous to drawing.

The forming limit diagram for a given material is developed by subjecting gauged specimens to a variety of loading conditions. After loading, strains to failure are plotted on the X-Y coordinate system of the forming limit diagram. Failure may be defined either as the formation of a localized neck or as fracture. For most applications, however, formation of a localized neck is the more useful criterion.

A notable feature of all forming limit diagrams is that the forming limit curve reaches a minimum at

a minor strain of zero (a loading condition known as plane strain). The generally accepted explanation for this behavior is that as a metal deforms, inhomogeneities (such as grinding marks, voids, or low cohesive strength inclusions) that lie parallel to the direction of major strain (e_1) greatly increase the rate of thinning in localized areas.[10] An obvious corollary is that as the ratio of minor to major strain (e_2/e_1) approaches 1, the region around a discontinuity will take longer to reach a condition of plane strain, and failure will occur at a higher overall strain level where other fracture mechanisms may be dominant.[8]

II. THE TEST PROGRAM

The primary objective of the biaxial test program was to generate sufficient data to permit accurate prediction of DOP-26 behavior in complex strain states, in short, to produce a forming limit diagram. Although the original test plan[11] was designed to investigate iridium behavior in a variety of strain states, strain rates, and temperatures, programmatic considerations limited the amount of DOP-26 iridium available for testing. Consequently, we developed a less ambitious test plan (Table I) to investigate alloy behavior at a single strain rate (punch velocity = 45 m/s) in near-plane-strain conditions. However, even the modified test plan required more test specimens than were available from a single batch of iridium powder.

Although all DOP-26 iridium sheet is fabricated from powder batches certified to be within a specific range of chemistry by Oak Ridge National Laboratory (ORNL), we felt that even minor batch-to-batch variations could affect the test results. Our solution, though less than ideal, was to test as many samples as possible from a single powder batch (Z-batch) and, whenever possible, to use specimens from other batches for setup and calibration purposes.

Midway through the modified test plan, ORNL completed development of a new process for fabricating DOP-26 iridium sheet. ORNL indicated that the new process significantly reduced fabrication costs and reject rates.[12] As part of the qualification procedure for the new process, we were asked to expand the biaxial testing program to include samples of new- and old-process material fabricated from a single batch of iridium powder. The new-process/old-process comparison (Table II) duplicated the most significant aspects of the original test plan (Table I) and investigated the material response at two additional temperatures (900°C and 1100°C).

A. Test Specimens

All of the test specimens used to complete the modified test plan and the new-process/old-process comparison were fabricated from DOP-26 iridium sheet of certified, acceptable chemical composition. Although the test specimens used to complete the modified test plan contained small defects that rendered them unusable for extraterrestrial applications, the defects were not located in the regions of greatest strain. The results obtained from these samples should be considered representative of Z-batch material.

In biaxial testing, variations in the loading condition (the strain state) are achieved by modifying the geometry of either the test specimen or the fixture used to cause deformation. Because the cost of machining punches was prohibitive, we chose to vary the imposed strain state by varying test specimen geometry. Plane strain deformation (positive major strain, zero minor strain) was simulated by stretching a 52-mm-diameter DOP-26 iridium disc over the surface of a hemispherical (31.75-mm-diameter) punch. Uniaxial tensile conditions (positive major strain, negative minor strain) were created by stretching 52-mm × 12.7-mm strips over the surface of the same punch. Thickness in all of the test specimens was 0.65 mm.

Table I. Modified Biaxial Test Plan[a,b]

Test Temperature (°C)	Strain State	Average g/t	No. of Specimens
1440	+,0	25	2
1440	+,−	25	2
1440	+,0	15	2
1440	+,−	15	2
1440	+,0	5	2
1000	+,0	25	2
1000	+,0	15	2
1000	+,0	5	2
800	+,0	25	2
800	+,0	15	2
600	+,0	25	2

[a]All specimens would be impacted at 45 m/s.
[b]Nominal thickness of 0.65 mm.

Table II. New-Process/Old-Process Comparison[a]

Test Temperature (°C)	Strain State	Average g/t	Material	Test Specimens
1440	+,0	25	New Proc.	2
1440	+,0	25	Old Proc.	2
1100	+,0	15	New Proc.	2
1100	+,0	15	Old Proc.	2
1000	+,0	25	New Proc.	2
1000	+,0	15	New Proc.	2
1000	+,0	25	Old Proc.	2
1000	+,0	15	Old Proc.	2
900	+,0	15	New Proc.	2
900	+,0	15	Old Proc.	2
800	+,0	15	New Proc.	2
800	+,0	15	Old Proc.	2

[a]All specimens would be impacted at 45 m/s.

B. Equipment

The punch tests were conducted in a 50.8-mm-bore, high-velocity gas gun (Fig. 2) designed to test specimens in vacuum. The gun used compressed nitrogen to accelerate a titanium-alloy punch to the desired impact velocity. Punch velocity was verified by means of several pins on the interior of the bore. The pins were connected to a weak electric current and insulated from contact with the gun; as the punch ran across and grounded each pin, a signal was generated. By analyzing the signal frequencies and by knowing the distance between pins, we could determine the punch velocity.

Each test specimen was held in a two-piece molybdenum-alloy (TZM) die centered in the gun bore. Punch penetration (strain in the test specimen) was controlled by modifying the length and diameter of a disposable brass sleeve placed over the punch. Both the TZM die set and the titanium-alloy punch (with sleeve) are shown in Fig. 3.

The test specimen was heated to temperature by a series of tungsten filaments (Fig. 4) that encircled the TZM die set. The filaments were resistance heated to high temperature and radiated heat to the die set; as the die set warmed, heat was conducted to the test specimen. Temperature of the die set was monitored by means of a calibrated thermocouple (tungsten-5 wt% Re vs. tungsten-26 wt% Re). When test temperatures in excess of 1200°C were required, the die set was electron-beam heated to temperature. The electron-beam heating was accomplished by connecting the die and tungsten filaments to a high-voltage power supply: the filaments were connected to ground, and the die set was connected to positive. When the electric potential between the die set and filaments was great enough, and if a vacuum of at least 10^{-4} torr had been achieved, the filaments emitted a stream of electrons that impacted and rapidly heated the die set.

C. Procedures

Before being tested, the surface of each specimen was marked with a circle-grid pattern (1.27-mm-diameter circles) so that the strains to failure could be easily measured. The grid pattern was produced by an eight-step photoresist process, a detailed explanation of which is given in Appendix A. The grid on an undeformed test disc may be seen in Fig. 5.

The test specimens were heat treated in vacuum to achieve the desired grain size. Three heat treatments

Table III. Grain-Sizing Heat Treatments

Nominal Grain Size/ 0.65 mm thickness	Heat Treatment	
	Temperature (°C)	Time (h)
25	1500	1
15	1500	18
5	1500	1
	1800	1

were used (Table III) to develop nominal grain sizes of 25, 15, and 5 grains/thickness (g/t).

After heat treatment, each test specimen was inserted into the TZM die set and centered in the bore of the 50.8-mm gas gun. The impact chamber was evacuated to 5×10^{-4} torr, and the tungsten heating elements were connected to a power supply. When the die set reached the desired test temperature, power to the heating elements was reduced to a level sufficient only to maintain temperature, thus allowing the temperatures of the die set and test specimen to equilibrate. After the die set had been at temperature for at least 5 min, the gun was fired.

We determined the local strains in each test specimen by measuring the deformation of the 1.27-mm-diameter circles marked on the sample surface. The measurement of a typical circle is illustrated in Fig. 6. Before measurement, each circle was classified as follows: (1) unaffected—uniform deformation with no evidence of localized necking or fracture (Fig. 7), (2) necked—the area within the circle contained a localized neck (Fig. 8), or (3) fractured—the area within the circle contained a crack (Fig. 9).

Note that no attempt was made to differentiate between penetrating and nonpenetrating cracks. We felt that the low toughness of iridium at most of the test temperatures required as strict an interpretation of fracture as possible, because even an infinitesimal increase in strain would cause a shallow crack to fully penetrate the iridium. We did, however, make an exception to this criterion for test specimens in which shallow grain boundary cracking (commonly referred to as orange peeling) occurred at low strains. Because the orange peeling occurred throughout each of the affected test specimens, its presence in a region of otherwise uniform deformation could not be considered indicative of impending failure.

After strain measurement, each test specimen was sectioned to provide samples for spectroscopic analysis, metallography, and electron microscopy.

III. RESULTS

The disposition of test specimens used to complete the modified and new-process/old-process comparison test plans is presented in Tables IV and V. Both tables also list the average grain size of each sample. Spectroscopic analyses of the test specimens are presented in Table VI.

Although the modified biaxial test plan (Table I) required a minimum of 18 DOP-26 discs to evaluate all of the test conditions, we had not anticipated that a number of discs would be required for setup purposes, that hardware problems would invalidate some tests, or that two test discs would not be adequate to fully evaluate the material response in some test conditions. Thus, we would have had too few discs to complete the plan. Fortunately, we began the test program by investigating the material properties at 1440°C and found that the coarse-grained material (nominally 5 g/t) had such low ductility that additional testing at lower temperatures was not necessary. Similarly, in our investigation of properties at 1000°C, we found that the ductility of the 15 g/t (nominal) material was already low enough to cause measurement problems.

The biaxial test results for each group of test specimens are summarized in the failure limit diagrams and in the data points used to construct each diagram (see Appendix B). The scarcity and scatter of data points in several of the failure limit diagrams reflect the limited number of test specimens; had more specimens been available, the failure curves would be much more clearly defined.

Although each test disc ideally provided a minimum of 700 data points (deformed circles), two factors rendered most of these readings as either insignificant or false. First, the mechanics of punch deformation dictated that the greatest amount of deformation in each disc would occur in a narrow ring of material (approximately 25% of the circle grid). Consequently, only a relatively small number of circles experienced strains sufficient to cause failure. In addition, once a failure had been initiated, it often propagated into adjoining lower-strain areas, thereby producing apparent evidence of low-strain-level failures. For most of the test conditions, these "false" failures could be screened out by comparing the apparent failure strains with the strains experienced by areas that had not failed. Unfortunately, however, because of a scarcity of data points in some test conditions, we did not have enough information to make this distinction, and therefore questionable (although conservative) failure readings were included in the failure limit diagram.

Table IV. Disposition of Specimens Used to Complete the Modified (Z-Batch) Biaxial Test Plan[a]

Specimen I.D.	Heat Treatment[b]	Geometry	Strain State	Test Temperature (°C)	Average g/t[c]
VR227–6	A	disc	+,0	1440	23.5
ZR566–3	A	disc	+,0	1440	24.9
ZR588–3	A	strip	+,–	1440	23.2
ZR588–6T	A	strip	+,–	1440	16.4
ZR576–1	B	disc	+,0	1440	10.0
ZR576–8[d]	B	disc	+,0	1440	11.3
ZR588–4	B	strip	+,–	1440	18.6
QR828–6	C	disc	+,0	1440	4.3
VR235–2	C	disc	+,0	1440	5.3
ZR572–1	C	disc	+,0	1440	5.8
Z563–5[d]	A	disc	+,0	1000	22.8
ZR576–5	A	disc	+,0	1000	25.9
ZR579R–5	A	disc	+,0	1000	24.3
RR932–2	B	disc	+,0	1000	15.3
RR932–6	B	disc	+,0	1000	11.5
Z561–6[d]	A	disc	+,0	800	22.5
ZR567–5	A	disc	+,0	800	24.9
Z563–2	A	disc	+,0	600	20.5
ZR576–3	A	disc	+,0	600	25.8

[a]All test specimens were impacted at 45 m/s.
[b]Three heat treatments were used to modify the iridium grain size:
A = annealed for 1 h at 1500°C.
B = aged for 18 h at 1500°C.
C = annealed for 1 h at 1500°C, then aged for 1 h at 1800°C.
[c]Nominal thickness of 0.65 mm.
[d]The disc was not tested to failure. After the first test, it was machined into a 20-mm-wide tensile specimen, which was tested to failure.

Plane strain failure limits derived from the failure limit diagrams are listed in Table VII. Because of the brittle/ductile behavior of DOP-26 iridium in the temperature range of interest, we were forced to use two definitions of failure. In the case of fine-grained material tested at 1440°C, we considered failure to be the formation of a localized neck. Although the material demonstrated considerable ductility at this test condition, we felt that once a localized neck developed it would quickly thin to failure with a negligible increase in macroscopic strain. For coarse-grained material, or for fine-grained specimens tested at lower temperatures where no localized necking was observed, we considered failure to be fracture of the iridium.

Because two criteria were used to define failure, two methods were used to determine the plane strain failure limits. For test conditions in which the iridium demonstrated significant ductility, failure strain was determined by first locating the highest strain reading

Table V. Disposition of Specimens Used for the New-Process/Old-Process Comparison[a]

Specimen I.D.	Material	Heat Treatment[b]	Strain State	Test Temperature (°C)	Average g/t[c]
B1-1-5	New Proc.	A	+,0	1440	22.7
B1-2-6	New Proc.	A	+,0	1440	22.3
B701-1	Old Proc.	A	+,0	1440	21.3
B701-2	Old Proc.	A	+,0	1440	22.7
B2-2-3	New Proc.	B	+,0	1100	12.8
B2-8-5	New Proc.	B	+,0	1100	11.4
B701-3	Old Proc.	B	+,0	1100	13.2
B727-4	Old Proc.	B	+,0	1100	16.2
B1-1-1	New Proc.	A	+,0	1000	23.3
B1-2-2	New Proc.	A	+,0	1000	18.8
B1-7-3	New Proc.	A	+,0	1000	19.5
B703-3	Old Proc.	A	+,0	1000	28.2
B704-1	Old Proc.	A	+,0	1000	22.7
B1-4-2	New Proc.	B	+,0	1000	14.0
B1-7-5	New Proc.	B	+,0	1000	11.8
B704-3	Old Proc.	B	+,0	1000	12.7
B704-4	Old Proc.	B	+,0	1000	12.8
B1-4-1	New Proc.	B	+,0	900	13.8
B2-1-2	New Proc.	B	+,0	900	11.2
B2-8-3	New Proc.	B	+,0	900	12.3
B703-2	Old Proc.	B	+,0	900	13.5
B732-5	Old Proc.	B	+,0	900	13.2
B2-2-4	New Proc.	B	+,0	800	14.4
B2-5-1	New Proc.	B	+,0	800	14.0
B729-2	Old Proc.	B	+,0	800	9.2
B731-1	Old Proc.	B	+,0	800	10.6

[a]All test specimens were in the form of discs and were impacted at 45 m/s.
[b]Two heat treatments were used to modify the iridium grain size:
A = annealed for 1 h at 1500°C.
B = aged for 18 h at 1500°C.
[c]Nominal thickness of 0.65 mm.

Table VI. Spectroscopic Analyses of the Biaxial Test Specimens[a]

Specimen I.D.	Selected Elements (ppm)								
	Fe	Al	Ca	Ni	Si	Cr	Mo	Cu	Pt
QR828-6	100	60	ND[b]	ND	15	10	ND	25	30
RR932-2	20	40	ND	20	30	40	1000	10	ND
RR932-6	10	60	ND	ND	20	10	ND	10	ND
VR227-6	40	60	3	ND	20	20	1000	20	ND
VR235-2	40	70	3	30	30	100	300	30	ND
Z561-6	30	70	ND	ND	ND	ND	ND	15	ND
Z563-2	30	50	ND	ND	ND	ND	ND	20	30
Z563-5	1000	80	5	ND	ND	10	ND	50	ND
ZR566-3	50	50	3	ND	ND	ND	ND	30	ND
ZR567-5	30	60	ND	ND	10	ND	ND	20	ND
ZR572-1	100	70	3	ND	50	10	ND	50	ND
ZR576-1	50	50	ND	ND	20	10	ND	50	ND
ZR576-3	70	70	ND	ND	30	10	ND	30	ND
ZR576-5	50	100	5	ND	100	15	ND	40	ND
ZR576-8	150	80	3	ND	60	10	300	30	30
ZR579R-5	30	80	ND	ND	60	ND	ND	20	ND
ZR588-3	100	80	3	ND	15	20	ND	60	ND
ZR588-4	30	50	ND	ND	15	ND	ND	60	ND
ZR588-6T	30	50	ND	ND	15	ND	ND	50	ND
B1-1-1	100	80	ND	20	10	20	300	40	ND
B1-1-5	120	80	3	ND	ND	10	ND	50	ND
B1-2-2	150	80	ND	80	ND	30	ND	50	ND
B1-2-6	120	80	ND	40	ND	20	ND	50	30
B1-4-1	80	80	3	50	10	15	ND	25	30
B1-4-2	100	100	3	50	10	15	ND	30	30
B1-7-3	150	100	3	40	ND	15	ND	15	30
B1-7-5	40	60	ND	15	ND	10	ND	10	ND
B2-1-2	30	80	ND	ND	ND	ND	ND	10	ND
B2-2-3	30	100	ND	ND	ND	ND	ND	20	ND
B2-2-4	40	100	3	ND	ND	ND	ND	20	ND
B2-5-1	50	80	ND	ND	ND	ND	ND	15	30
B2-8-3	50	80	ND	10	ND	ND	ND	15	ND
B2-8-5	30	80	ND	ND	ND	ND	ND	6	ND
B701-1	ND	100	ND	ND	30	ND	ND	10	ND
B701-2	ND	150	ND	ND	30	ND	ND	10	ND
B701-3	ND	150	ND	ND	30	ND	ND	10	ND
B703-2	ND	70	ND	ND	ND	ND	ND	10	ND
B703-3	ND	80	ND	ND	ND	ND	ND	15	ND
B704-1	ND	100	ND	ND	ND	ND	ND	15	ND
B704-3	ND	80	ND	ND	ND	ND	ND	30	ND
B704-4	ND	80	ND	ND	ND	ND	ND	30	ND
B727-4	40	100	ND	ND	ND	ND	ND	20	ND
B729-2	50	80	ND	100	ND	10	ND	15	ND
B731-1	50	60	ND	40	10	ND	ND	6	ND
B732-5	50	60	ND	20	ND	ND	300	6	ND

[a]Elements are listed only if they exceed the detectability limit in at least one specimen.
[b]None detected.

Table VII. Estimated Plane Strain Failure Limits

Material	Temperature (°C)	Nominal g/t	Failure Limit (% Major Strain)
Z-batch	1440	5	14
Z-batch	1440	15	53
Z-batch	1440	25	50[a]
B-batch (old)	1440	25	66[a]
B-batch (new)	1440	25	71[a]
B-batch (old)	1100	15	44
B-batch (new)	1100	15	51
Z-batch	1000	15	33
B-batch (old)	1000	15	37
B-batch (new)	1000	15	41
Z-batch	1000	25	47
B-batch (old)	1000	25	55
B-batch (new)	1000	25	57
B-batch (old)	900	15	24
B-batch (new)	900	15	27
B-batch (old)	800	15	17
B-batch (new)	800	15	15[b]
Z-batch	800	25	32
Z-batch	600	25	11

[a]The failure criteria applied to this test condition considered localized necking as equivalent to failure.
[b]Very few data points exist for this test condition.

(major strain) for uniformly deformed material within 5% minor strain of the major strain axis and then drawing a line with a slope of 1 from this point to intersect the major strain axis. The point of intersection with the major strain axis was considered the failure limit. For test conditions in which the iridium exhibited brittle behavior, failure strain was determined by first locating the highest failure reading within 5% of the major strain axis and then drawing an intersect line with a slope of 1 from this point to the major strain axis. The intersect line is given a slope of 1 in both methods, because we felt this would provide a reasonable estimate of the true failure strain; the slopes of failure limit curves for materials such as aluminum and steel typically range from 0.4 to 1.5 within 5% minor strain of the major strain axis.[8]

The fracture surfaces of selected test specimens are shown in Figs. 10–19. Microstructures of typical ductile (specimen VR227-6) and brittle (specimen RR932-2) failures may be seen in Figs. 20 and 21.

IV. DISCUSSION

A. General

The results indicate that although the failure strengths of Z- and B-batch old-process and B-batch

new-process iridium differed significantly, the relationships between ductility and temperature, and between ductility and grain size, remained essentially the same for all three sample groups. As Fig. 22 illustrates, all of the fine-grained test specimens exhibited considerable ductility at 1440°C and were suprisingly brittle at temperatures as high as 1000°C. The absence of detectable localized necking in fine-grained specimens tested at 1000°C (Fig. 13) is particularly notable when contrasted with the plasticity of similar specimens tested at 1440°C (Fig. 10). The replication of this behavior in all three sample groups suggests it is an intrinsic characteristic of the DOP-26 alloy. Although the temperature dependence of alloy ductility does not appear to be a classic ductile/brittle transition, strain to failure at 1000°C cannot be related (linearly or otherwise) to failure strain at 1440°C (Fig. 22). The scope of this study was not wide enough to determine if a precise transition temperature exists or to identify the mechanism(s) responsible for the differences in high- and low-temperature ductility.

Another feature common to test specimens from all three sample groups was a tendency toward nearly exclusive intergranular failure. Although some fracture surfaces showed evidence of occasional intragranular cleavage (Figs. 13 and 17), even fine-grained specimens tested at 1440°C appeared to have failed by grain boundary fracture, albeit after considerable grain elongation (Figs. 10 and 20). No evidence of recrystallization was observed in any of the specimen microstructures (Fig. 20). The short time at temperature and the elevated strain rate apparently prevented appreciable recrystallization. We did not perform any transmission electron microscopy of test specimen foils; consequently, the extent to which recovery processes, such as polygonization or subgrain development, occurred at the various test temperatures is unknown.

An interesting phenomenon observed in several test specimens was an association between grinding marks on the metal surface and crack initiation. As Fig. 23 illustrates, the grinding marks apparently were stress concentrators. Small cracks initiated in the troughs of the grinding marks and then propagated normal to the direction of major strain. This phenomenon was only observed in low-ductility specimens; the ductility and toughness of the fine-grained material tested at 1440°C would probably minimize the stress-concentrating effects of any surface defect.

We do not know the comprehensive effect of the grinding marks on the failure limit data generated in this study. However, the presence of the grinding marks obviously can only degrade material performance. A second and perhaps more important unknown is how the data generated in this study relate to the deformation of DOP-26 iridium capsules, which have a grit-blasted outer surface. In more forgiving materials such as aluminum or steel, one would expect grit-blasting to raise the failure strain by peening out the sharp edges of surface defects and by producing a residual state of compressive stress in the outer surface of the metal. In DOP-26 iridium, however, the effects of grit-blasting are unknown.

B. Z-Batch Test Results

Spectroscopic analyses (Table VI) of the test specimens did not identify any significant differences in chemistry between Z-batch iridium and Q-, R-, or V-batch material. Although the analyses indicate that specimens VR227-6 and RR932-2 contained 1000 ppm of molybdenum, these values are anomalous and probably result from sampling or analytical errors. None of the other V- and R-batch test specimens contained comparable levels of molybdenum. In addition, the detection limit for molybdenum is relatively high (300 ppm). The excessive iron content (1000 ppm) detected in specimen Z563-5 should also be considered an anomaly; the iron content of all other Z-batch test specimens ranged from 10 to 150 ppm.

Unfortunately, we had too few test specimens to develop clearly defined failure limits for some test conditions, but the most serious result of having too few data points is probable underestimation of strain to failure. Failures resulting from crack propagation into low-strain areas can only be disregarded after numerous data points for the same condition of minor strain have been recorded.

The test results indicate that the mechanical properties of Q-, V-, and Z-batch iridium are approximately equivalent. In test conditions where Q- or V-batch specimens were paired with Z-batch specimens, no significant differences in mechanical response were observed. Because only R-batch specimens were tested in the 1000°C, 15 g/t condition, no direct comparison of R- and Z-batch properties is possible. However, comparing the R-batch results with the behavior of Z-batch material in other test conditions suggests that R- and Z-batch properties are not dissimilar. Consequently, for the purposes of this study we considered Q-, V-, and R- batch material as equivalent to Z-batch iridium.

The response of the iridium to heat treatment was not as consistent as the mechanical response.

Although no obvious differences in the grain sizes of similarly treated Q-, R-, V-, or Z-batch test specimens were apparent, anomalous grain sizes were observed in two Z-batch specimens. After being heat treated for 1 h at 1500°C, specimen ZR588-6T contained an average of only 16.4 g/t; other test specimens given the same heat treatment averaged 23.8 g/t. The other grain size anomaly was in specimen ZR588-4, which contained an average of 18.6 g/t after being heat treated for 18 h at 1500°C; other test specimens given the same aging treatment averaged 12.0 g/t.

The simplest explanation for the anomalous grain size of samples ZR588-6T and ZR588-4 would be improper heat treatment. However, all test specimens were heat treated inside a thermostatically controlled furnace that continuously recorded temperature on a strip chart; no unusual temperature excursions occurred during the heat treatment of ZR588-6T or ZR588-4. A second, perhaps more likely, explanation is that the metallographic section obtained from each specimen happened to be located in an unusually coarse- (ZR588-6T) or fine-grained (ZR588-4) area. In support of this hypothesis, the mechanical responses of both specimens were consistent with the behavior of other specimens given the same heat treatments.

C. New-Process/Old-Process Comparison

Spectroscopic analyses (Table VI) of the new- and old-process test specimens did not reveal any significant differences between the two sample groups. Although the iron contents of the old-process test specimens (which ranged from the detection limit to 50 ppm) were generally lower than those of the new-process specimens (which ranged from 30 to 150 ppm), these small differences probably did not affect mechanical behavior.

Metallographic examination of the new- and old-process test specimens did not identify any significant microstructural differences. No defects were observed in any of the test specimens, and the response to heat treatment appeared similar for both sample groups. Of the materials annealed for 1 h at 1500°C, the new-process specimens contained an average of 21.3 g/t, and the old-process specimens averaged 23.7 g/t. Of materials aged for 18 h at 1500°C, the new-process specimens contained an average of 12.9 g/t, whereas the old-process specimens averaged 12.7 g/t.

Because of our experience with the Z-batch material, we were able to complete the new-process/old-process comparison without sacrificing any specimens as setup pieces. In addition, because the Z-batch test results established an optimum punch penetration for each test condition, we generally were able to obtain more useful data points per test than had been the case previously.

The biaxial results indicate that the new-process iridium was slightly more ductile than the old-process material. However, the limited number of test specimens makes it difficult to determine whether the ductility of the new-process material was significantly (on a statistical basis) better than that of the old-process material. In addition, the new-process/old-process comparison was weighted toward relatively low-temperature test conditions, where the ductility of both new- and old-process material was low and differences in ductility were difficult to detect.

The most likely explanation for the apparent superiority of the new-process material is that the new fabrication process significantly reduces the number and size of defects in the iridium sheet. Although no microstructural defects were observed in any of the test specimens, a small defect in a highly strained area is all that would be required to initiate a premature failure.

Another reason for the improved ductility of the new-process material might be that the new production process imparts a beneficial crystallographic texture into the iridium sheet. Or, the new production process may prevent the formation of a detrimental texture that may have been present in sheet produced by the old method. Because we did not include x-ray diffraction studies in our evaluation of the material performance, we could not determine the extent to which crystallographic textures may or may not be present.

D. B-Batch/Z-Batch Comparison (Old Process)

The biaxial test results indicate that the ductility of B-batch (old-process) test specimens was significantly greater than that of similarly processed Z-batch specimens. For each test condition where a direct comparison is possible, the failure limit (Table VII) of B-batch iridium is at least 10% higher than that of the Z-batch material. Although the Z-batch test specimens (discs) had originally been designated as "non-flight-quality" because they contained small defects, these defects were not generally located in high-strain areas (the size and location of defects in each disc were documented by ORNL) and did not appear to have

initiated any specimen failures. The reduced ductility of the Z-batch test specimens is apparently related to alloy chemistry, microstructure, or the presence of previously undetected defects.

Spectroscopic analyses (Table VI) of old-process Z- and B-batch test specimens did not reveal any significant differences in chemistry. However, the effects of trace elements (excluding thorium) on the mechanical properties of DOP-26 iridium are not well understood. Consequently, while small differences in chemical composition may appear to be insignificant, the effect of these differences on mechanical response may in fact be profound.

Metallographic examination of the Z- and B-batch test specimens revealed that the response to heat treatment was essentially the same for both sample groups. However, delamination-type defects (Fig. 24) were observed in several of the Z-batch test specimens. Although this type of defect generally does not affect ductility, a complex strain state, perhaps created through the interaction of adjacent defects, can greatly alter the behavior of any inhomogeneity. Because no similar defects were observed in any of the B-batch test specimens, we must consider that delamination defects may be at least partially responsible for the reduced ductility of the Z-batch material. Another, and perhaps more likely, possibility is that while the delamination defects did not themselves cause crack initiation, their presence indicates that the material may have also contained other, more damaging defects.

V. CONCLUSIONS

1. The B-batch test results indicate that the new-process iridium alloy was slightly more ductile than the old-process material.

2. The results also indicate that old-process B-batch test specimens were significantly more ductile than old-process Z-batch specimens.

3. The fracture strain of fine-grained (>20 grains/0.65-mm thickness) DOP-26 iridium is temperature dependent and may be affected by a ductile/brittle transition between 1000°C and 1440°C.

4. Even at temperatures as high as 1440°C, ductile fracture is apparently not possible in DOP-26 iridium that has coarsened to some critical grain size (perhaps between 15 and 20 grains/0.65-mm thickness).

VI. RECOMMENDATIONS

1. Additional specimens should be biaxially tested to determine whether surface modifications such as electropolishing or grit blasting increase the strain to failure.

2. An investigation should be initiated to determine what (if any) crystallographic textures are produced by the new and old processing methods, and to evaluate the effects of these textures, if they are found to exist.

3. Additional specimens should be tested in the 1100°C–1800°C temperature range to determine if a precise ductile/brittle transition temperature for fine-grained DOP-26 iridium exists, and to determine whether coarse-grained material can be made to fail in a ductile manner.

4. A small number of discs (or fabricated cups) should be sectioned and metallographically examined to determine the range of grain sizes that may be present.

ACKNOWLEDGMENTS

I would like to thank the following for their valuable assistance: M. Anstey, C. Frantz, and A. Herrera for conducting the biaxial tests and handling all of the problems associated with this activity; S. Hecker, for allowing me to examine his notes on the biaxial testing done during development of the DOP-26 alloy; Jose Archuleta for his excellent metallography and his SEM expertise; and R. Henneke for helping us improve the gridding process.

REFERENCES

1. F. W. Schonfeld, "General-Purpose Heat Source Development: Safety Test Program, Postimpact Evaluation, Design Iteration Test 1," Los Alamos National Laboratory report LA-9680-SR (April 1984).

2. F. W. Schonfeld and T. G. George, "General-Purpose Heat Source Development: Safety Test Program, Postimpact Evaluation, Design Iteration Test 2," Los Alamos National Laboratory report LA-10012-SR (June 1984).

3. F. W. Schonfeld and T. G. George, "General-Purpose Heat Source Development: Safety Test Program, Postimpact Evaluation, Design Iteration Test 3," Los Alamos National Laboratory report LA-10034-SR (July 1984).

4. T. G. George and F. W. Schonfeld, "General-Purpose Heat Source Development: Safety Test Program, Postimpact Evaluation, Design Iteration Test 4," Los Alamos National Laboratory report LA-10217-SR (December 1984).

5. T. G. George and F. W. Schonfeld, "General-Purpose Heat Source Development: Safety Test Program, Postimpact Evaluation, Design Iteration Test 5," Los Alamos National Laboratory report LA-10232-SR (December 1984).

6. S. P. Keeler, "Circular Grid System—A Valuable Aid for Evaluating Sheet Metal Formability," Society of Automotive Engineering Congress, Paper 680092, January 1968.

7. G. M. Goodwin, "Application of Strain Analysis to Sheet Metal Forming Problems in the Press Shop," Society of Automotive Engineering Congress, Paper 680093, January 1968.

8. A. K. Ghosh, "The Influence of Strain Hardening and Strain-Rate Sensitivity on Sheet Metal Forming," Journal of Engineering Materials, July 1977, 264–274.

9. S. S. Hecker, "Simple Technique For Determining Forming Limit Curves," Sheet Metal Industries, November 1975, 671–676.

10. Z. Marciniak and K. Kuczynski, "Limit Strains in the Process of Stretch-Forming Sheet Metal," International Journal of Mechanical Sciences, Vol. 9, (1967), 609–620.

11. Memorandum from S. E. Bronisz to G. Bennet, "Iridium (DOP-26) Ductility, Biaxial Failure Limits Test Plan," March 28, 1983.

12. R. L. Heestand, G. L. Copeland, and M. M. Martin, "A Consumable Arc-Melting, Extruding, and Rolling Process for Iridium Sheet," Oak Ridge National Laboratory report ORNL-6270 (June 1986).

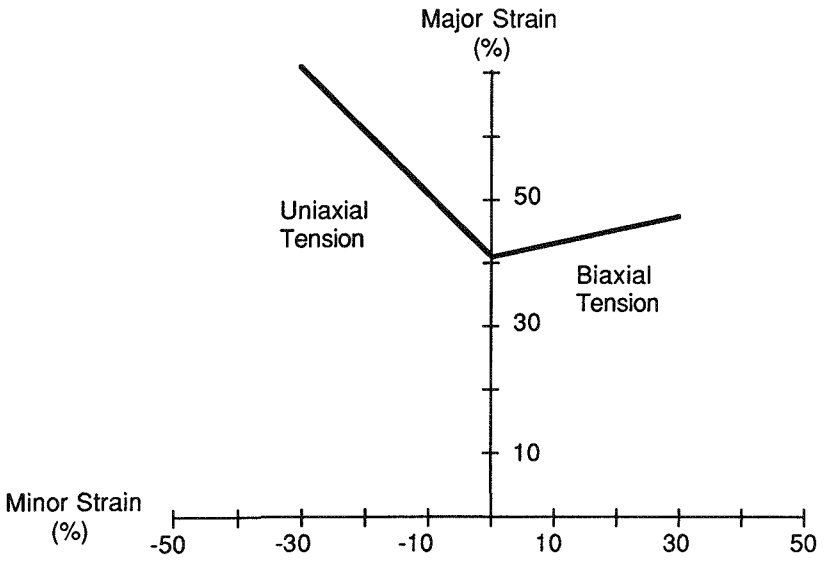

Fig. 1. A forming limit diagram depicts the effect of loading condition on strain to failure.

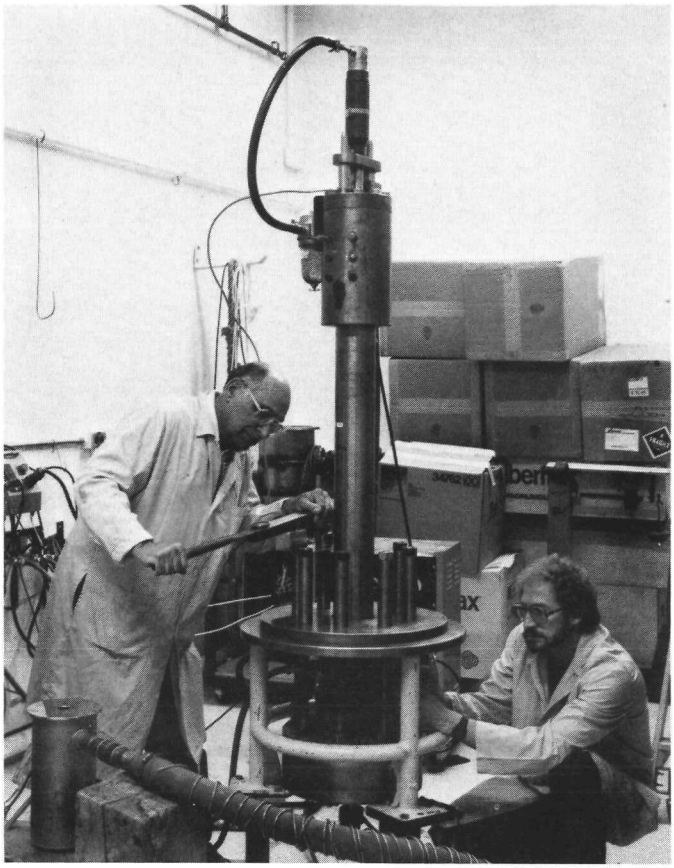

Fig. 2. The punch tests were conducted in a high-velocity gas gun.

Fig. 3. Each test specimen was held in a two-piece molybdenum-alloy die (at right) and was impacted by a titanium-alloy punch (left).

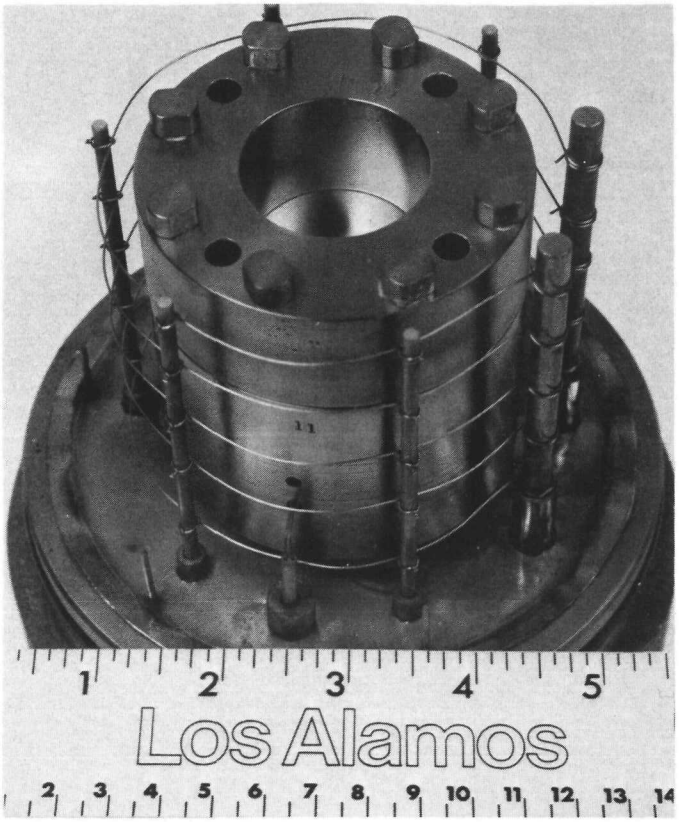

Fig. 4. The test specimen was heated by a series of tungsten filaments that encircled the die set.

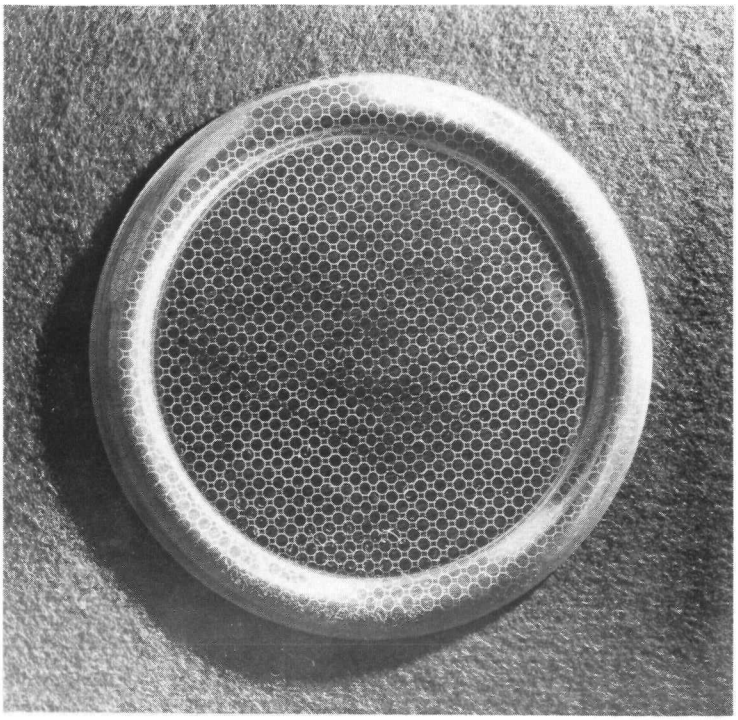

Fig. 5. A circle grid was grit-blasted onto the surface of each test specimen.

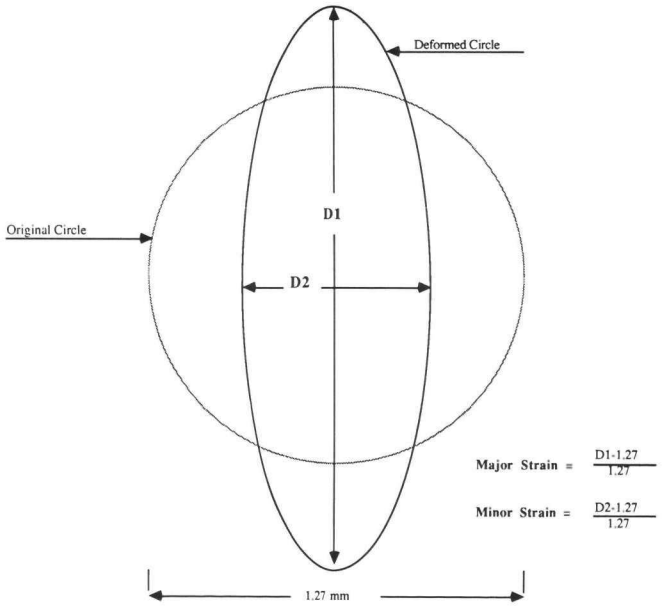

Fig. 6. Local strains were determined by measuring deformation of the 1.27-mm circles on the sample surface.

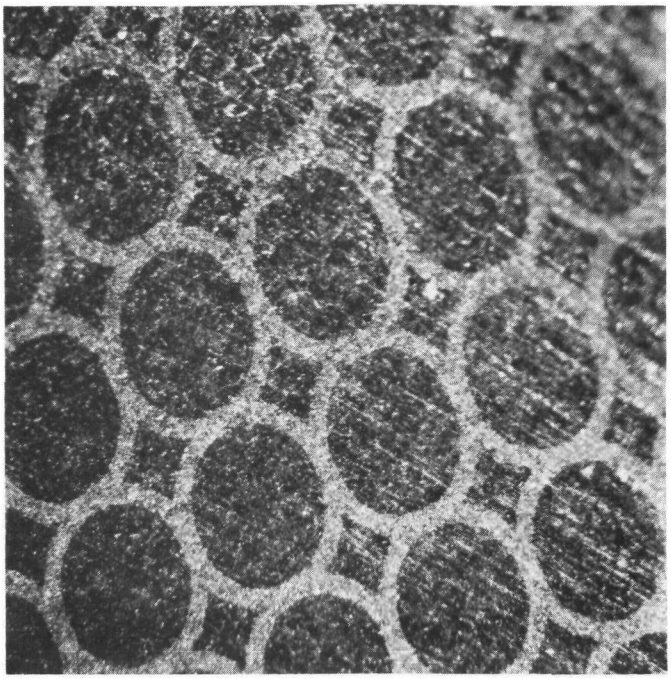

Fig. 7. An unaffected circle (no evidence of necking or fracture).

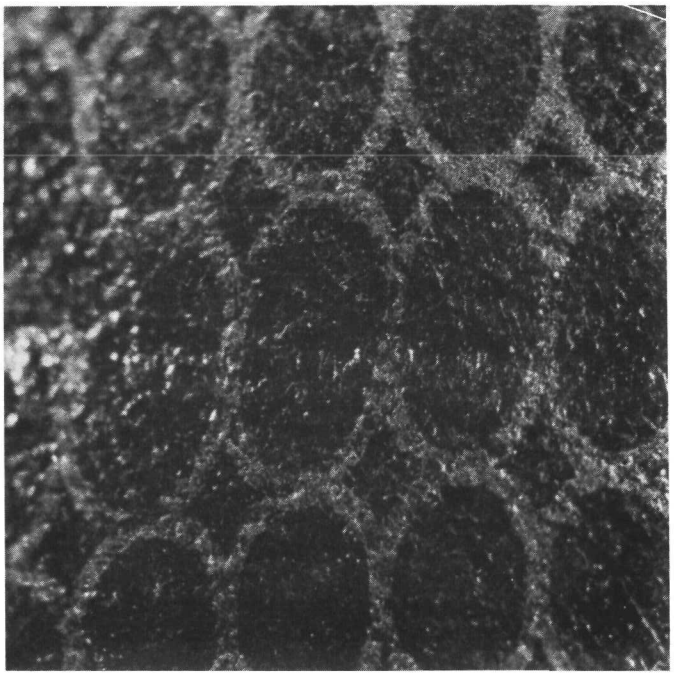

Fig. 8. A necked circle.

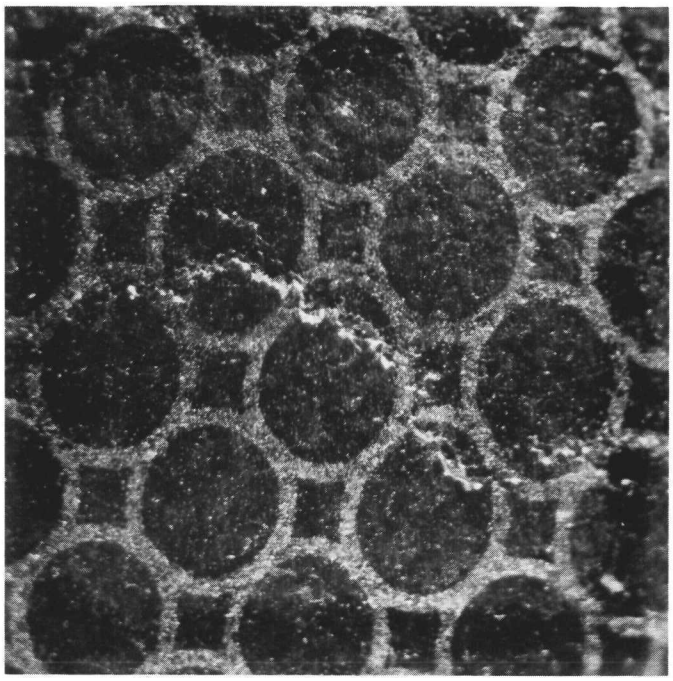

Fig. 9. A fractured circle.

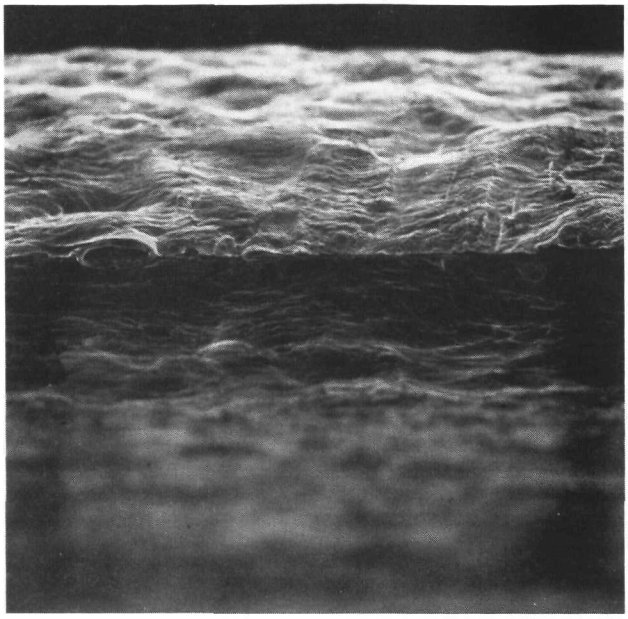

(a)

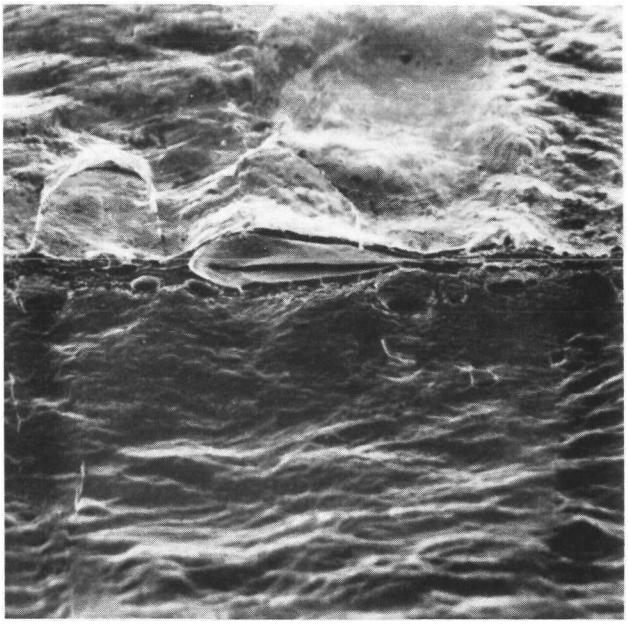

(b)

Fig. 10. Sample B1-2-6 (average 22.3 g/t, tested at 1440°C) necked down to a knife edge and displayed numerous voids along the fracture line. (a) Electron micrograph, 100X; and (b) electron micrograph, 500X.

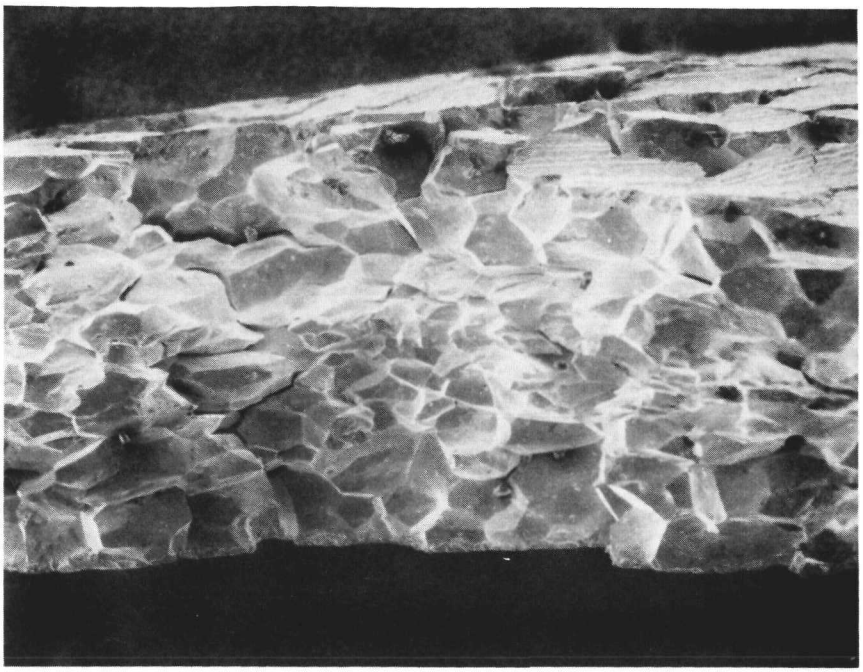

Fig. 11. Sample ZR576-1 (average 10.0 g/t, tested at 1440°C) failed in a very brittle manner; electron micrograph, 100X.

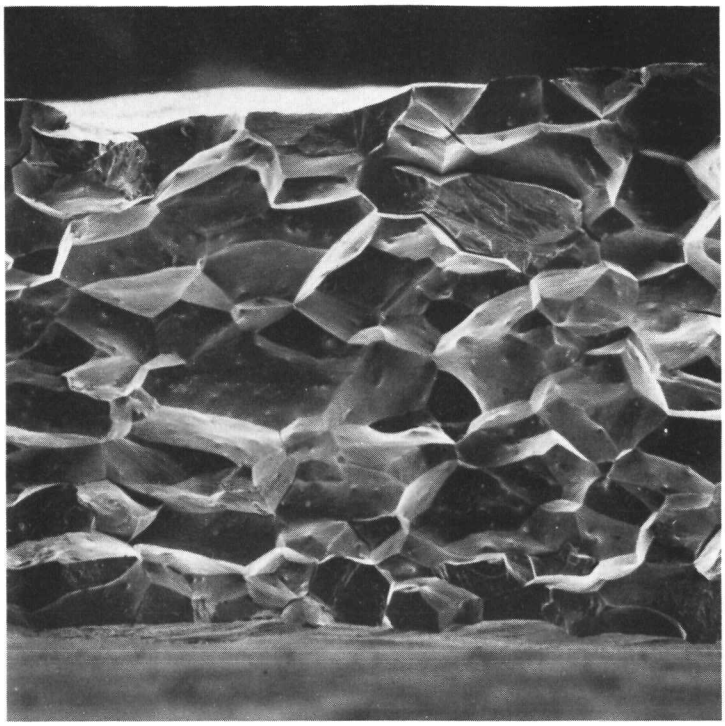

Fig. 12. Sample B2-8-5 (average 11.4 g/t, tested at 1100°C) also behaved in a brittle manner, with near-exclusive intergranular failure; electron micrograph, 100X.

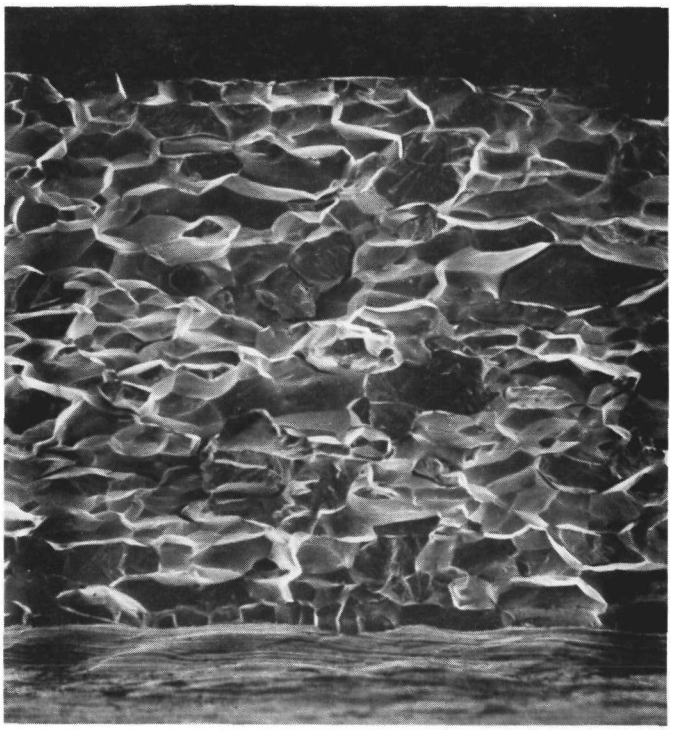

(a)

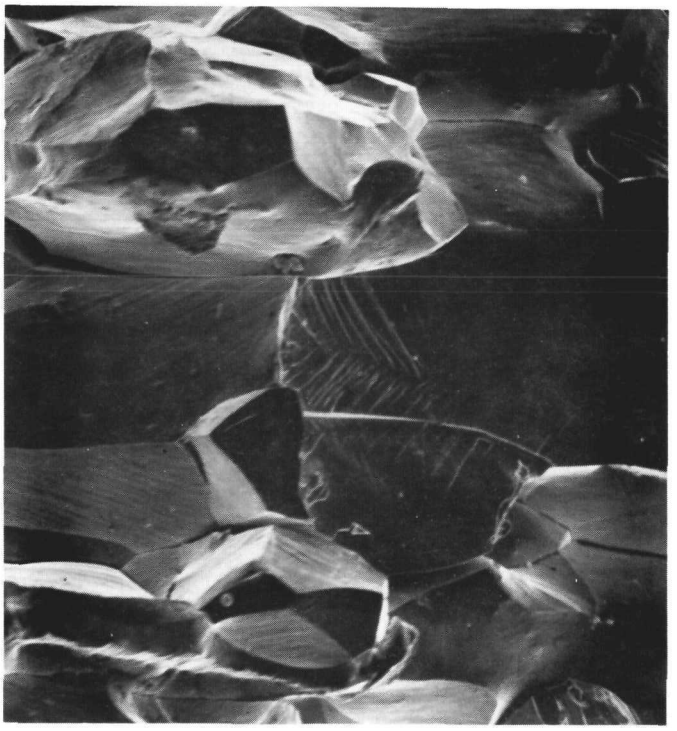

(b)

Fig. 13. Although the failure of sample B1-7-3 (average 19.5 g/t, tested at 1000°C) appeared to be almost entirely intergranular, isolated examples of grain cleavage were observed. (a) Electron micrograph, 100X; and (b) electron micrograph, 500X.

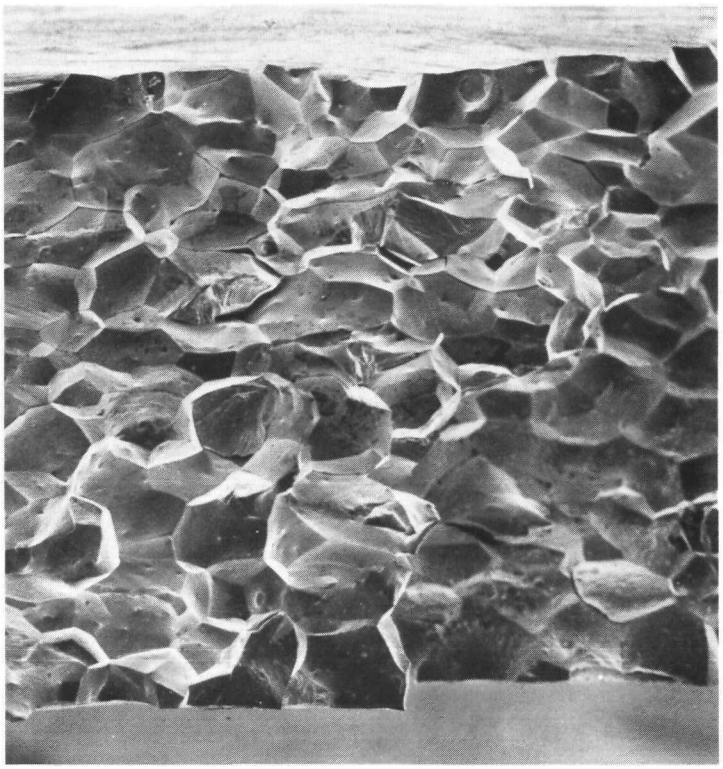

Fig. 14. Sample B1-4-2 (average 14.0 g/t, tested at 1000°C) failed in a brittle manner; electron micrograph, 100X.

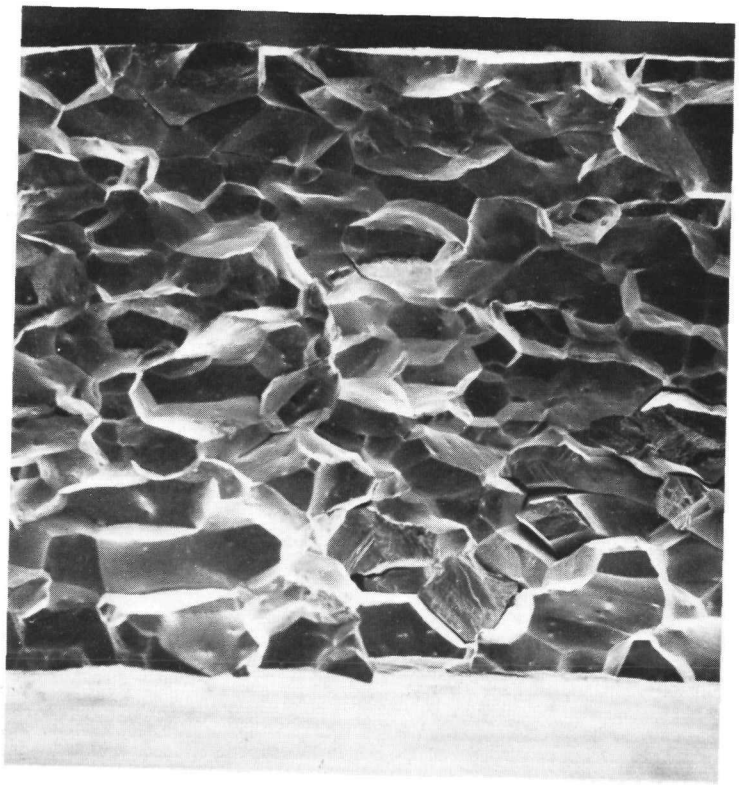

Fig. 15. Sample B2-8-3 (average 12.3 g/t, tested at 900°C) failed in a brittle manner, with little reduction in area; electron micrograph, 100X.

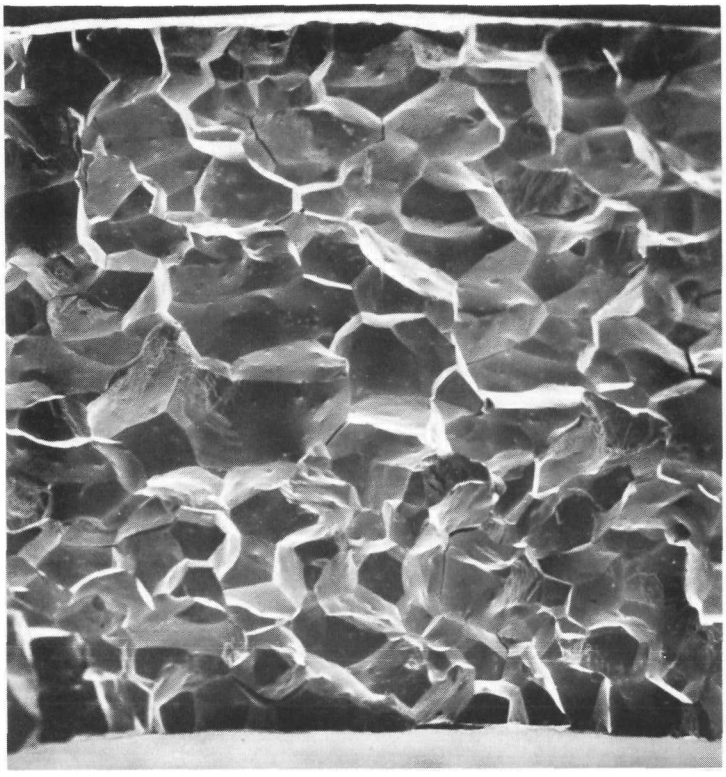

Fig. 16. The fracture surface of B2-2-4 (average 14.4 g/t, tested at 800°C) also had a brittle appearance; electron micrograph, 100X.

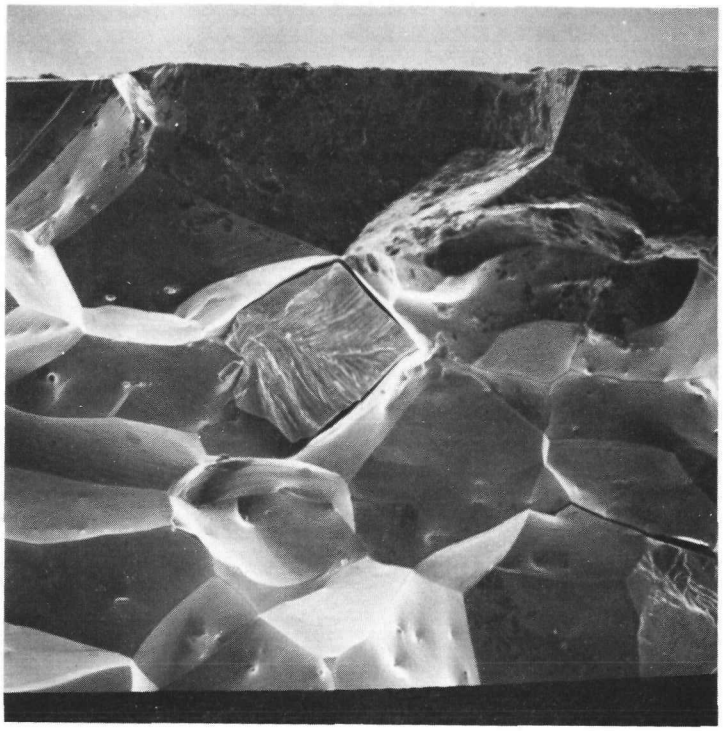

Fig. 17. Isolated examples of intragranular cleavage were observed on the surface of B2-5-1 (average 14.0 g/t, tested at 800°C). Electron micrograph, 300X.

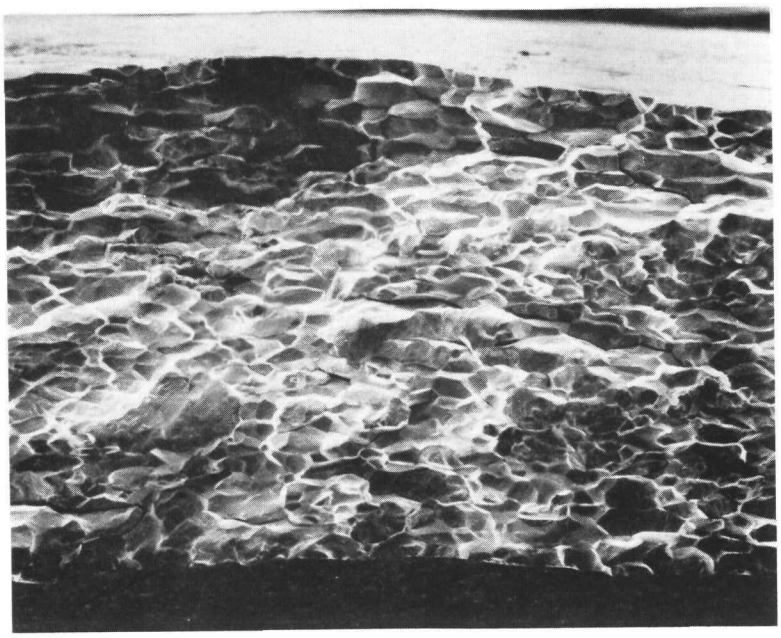

Fig. 18. Sample ZR567-5 (average 24.9 g/t, tested at 800°C) failed in a brittle manner; electron micrograph, 100X.

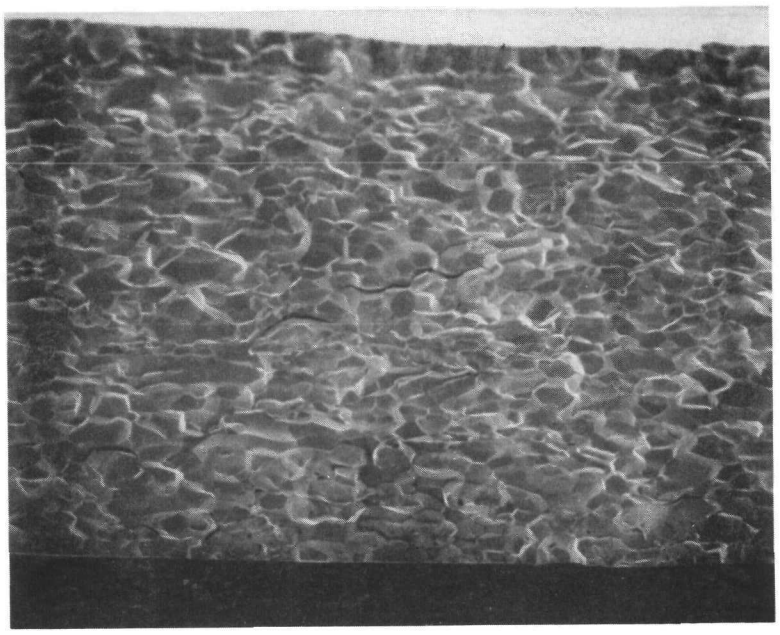

Fig. 19. Sample ZR576-3 (average 25.8 g/t, tested at 600°C) also had a brittle appearance; electron micrograph, 100X.

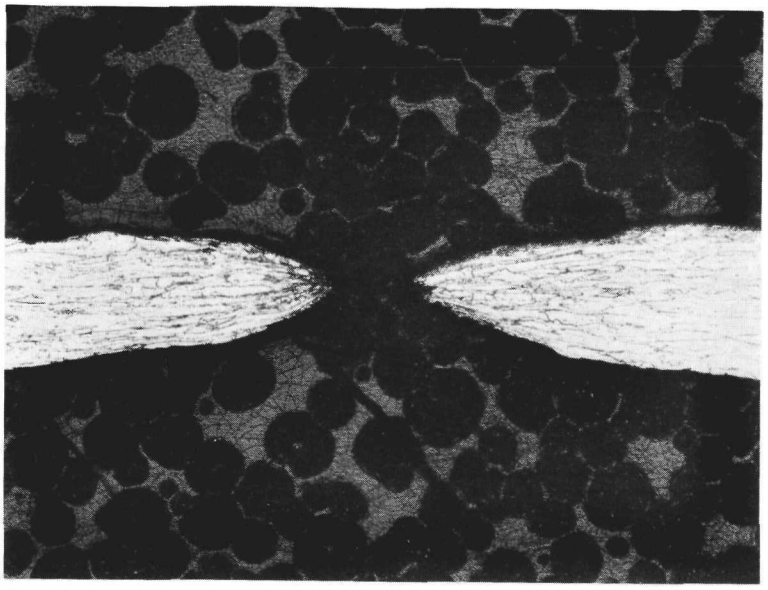

Fig. 20. No evidence of recrystallization was observed in any of the specimen microstructures. Sample VR227-6 (average 23.5 g/t, tested at 1440°C; etched, 50X.

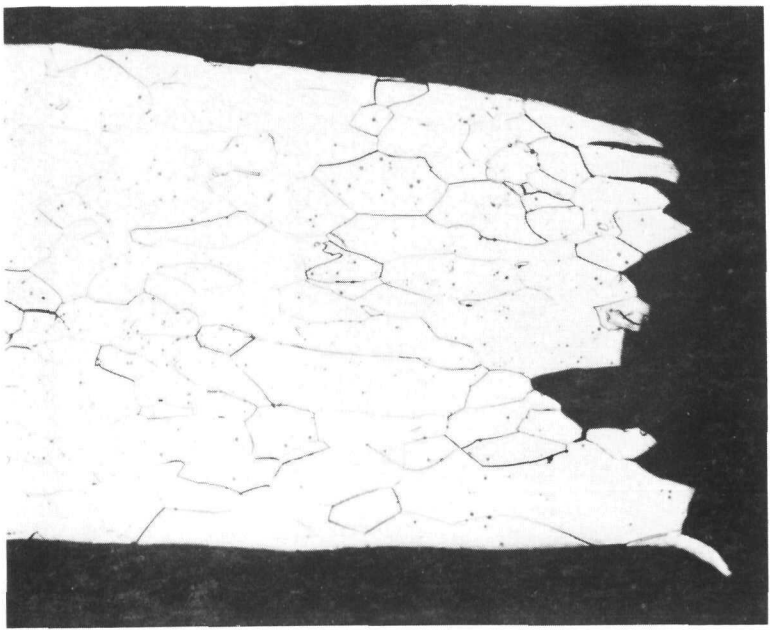

(a)

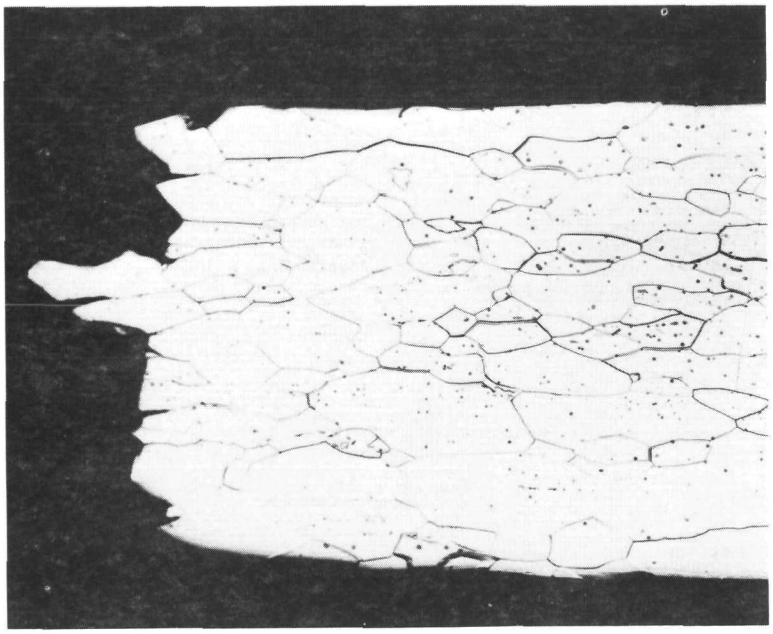

(b)

Fig. 21. Most of the specimens failed in a brittle manner, with negligible reduction in area. Sample RR932-2 (average 15.3 g/t, tested at 1000°C); (a) and (b) etched and at 100X.

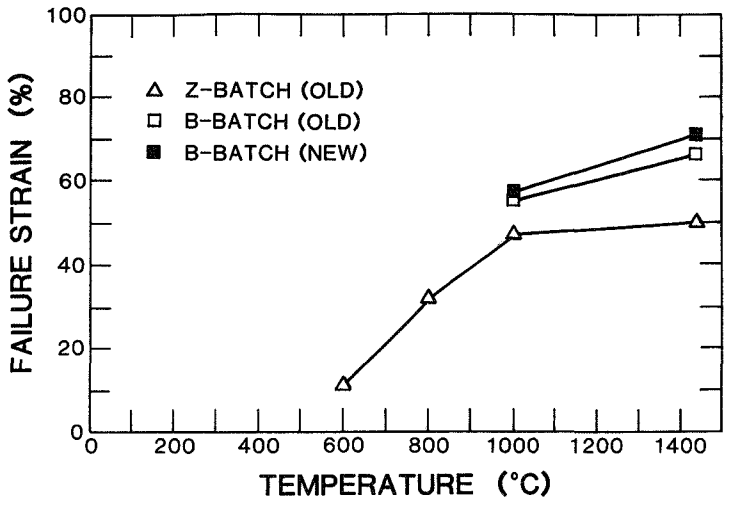

(a)

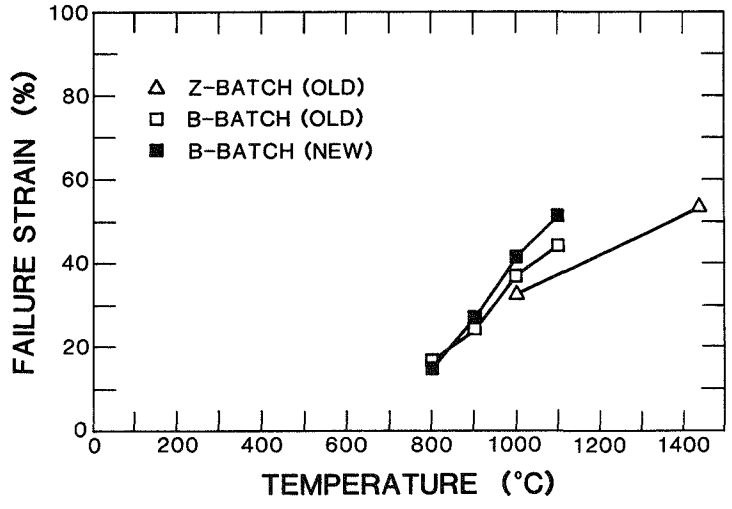

(b)

Fig. 22. The ductility of DOP-26 iridium is temperature dependent; (a) behavior of 25 g/t specimens and (b) behavior of 15 g/t specimens.

(a)

(b)

Fig. 23. Grinding marks on the metal surface may have acted as stress concentrators that caused premature failure. Sample ZR576-5; (a) electron micrograph, 50X, and (b) electron micrograph, 75X.

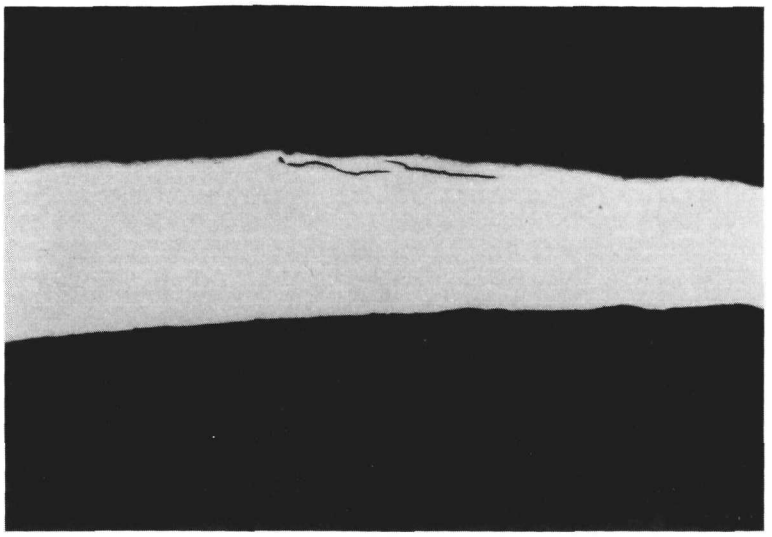

Fig. 24. Delamination defects were observed in several Z-batch test specimens. Sample VR227-6; as polished, 50X.

APPENDIX A

Photoresist Gridding Process

Step (1): Deposit (by physical vapor deposition) a 0.025-mm copper coating onto the metal surface.

Step (2): Apply a photosensitive resist over the copper coating.

Step (3): Expose the resist with the image of a circle grid.

Step (4): Immerse the specimen in a developer solution (to remove the resist from unexposed areas).

Step (5): Immerse the specimen in a nitric acid solution (to remove the copper coating from areas not covered by resist).

Step (6): Carefully grit-blast the sample surface with 10-μm alumina grit (to "frost" the metal surface in areas not covered by copper).

Step (7): Immerse the specimen in acetone (to remove all traces of the resist).

Step (8): Immerse the specimen in a nitric acid solution (to remove the remaining copper).

APPENDIX B

The Failure Limit Diagrams and the Data Points Used to Construct the Diagrams

Table B-I. Data Points Presented in Fig. B-1 (Z-Batch Specimens, Nominal 5 g/t, Tested at 1440°C)

Sample	Minor Strain (%)	Major Strain (%)	Condition
QR828-6	−1.0	13.5	Fractured
QR828-6	−0.5	8.0	Fractured
QR828-6	−3.5	9.5	Unaffected
QR828-6	−2.0	10.0	Unaffected
QR828-6	−1.5	7.5	Unaffected
QR828-6	−1.0	8.5	Unaffected
VR235-2	−1.0	14.0	Unaffected
QR828-6	0.0	10.5	Unaffected
VR235-2	0.5	12.0	Unaffected
ZR572-1	3.0	14.5	Unaffected
ZR572-1	4.0	12.0	Unaffected
ZR572-1	4.0	16.0	Unaffected
VR235-2	5.0	18.5	Unaffected
VR235-2	6.5	16.0	Unaffected

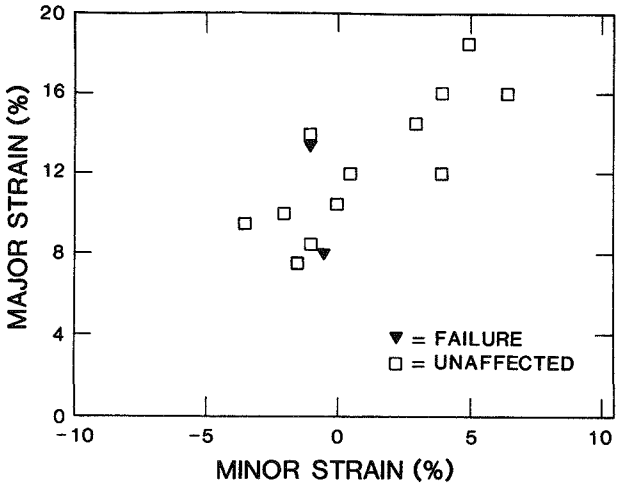

Fig. B-1. Failure limit diagram for Z-batch old-process specimens with a nominal grain size of 5 g/t, tested at 1440°C.

Table B-II. Data Points Presented in Fig. B-2 (Z-Batch Specimens, Nominal 15 g/t, Tested at 1440°C)

Sample	Minor Strain (%)	Major Strain (%)	Condition
ZR588-4	−13.5	77.5	Fractured
ZR588-4	−11.0	92.0	Fractured
ZR576-8	− 5.0	41.0	Fractured
ZR576-8	− 4.0	40.5	Fractured
ZR588-4	−14.5	40.5	Unaffected
ZR588-4	−12.0	35.0	Unaffected
ZR588-4	− 9.5	34.5	Unaffected
ZR588-4	− 6.0	36.5	Unaffected
ZR576-1	− 4.0	24.0	Unaffected
ZR588-4	− 2.0	54.5	Unaffected
ZR576-1	1.5	25.5	Unaffected
ZR576-1	3.0	23.5	Unaffected
ZR576-1	9.5	26.0	Unaffected

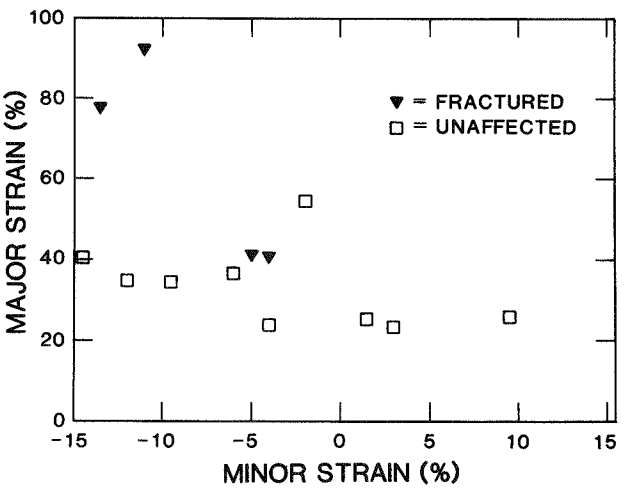

Fig. B-2. Failure limit diagram for Z-batch old-process specimens with a nominal grain size of 15 g/t, tested at 1440°C.

Table B-III. Data Points Presented in Fig. B-3 (Z-Batch Specimens, Nominal 25 g/t, Tested at 1440°C)

Sample	Minor Strain (%)	Major Strain (%)	Condition
ZR588-6T	−11.0	107.0	Fractured
VR227-6	2.5	114.0	Fractured
VR227-6	4.5	119.0	Fractured
VR227-6	8.0	118.0	Fractured
VR227-6	10.5	126.0	Fractured
VR227-6	12.5	122.0	Fractured
ZR588-3	−12.5	61.5	Necked
ZR588-6T	−11.0	66.5	Necked
ZR588-6T	− 9.0	56.5	Necked
ZR588-3	− 8.0	76.0	Necked
ZR588-6T	− 6.0	56.0	Necked
ZR588-3	− 3.0	68.5	Necked
ZR566-3	− 2.5	53.0	Necked
ZR566-3	− 0.5	54.5	Necked
ZR566-3	− 0.5	79.5	Necked
ZR566-3	1.0	52.0	Necked
VR227-6	2.0	65.5	Necked
ZR566-3	2.0	73.0	Necked
VR227-6	3.5	55.5	Necked
VR227-6	3.5	87.0	Necked
ZR566-3	4.5	60.5	Necked
VR227-6	5.5	100.0	Necked
ZR566-3	6.0	58.5	Necked
VR227-6	6.5	61.5	Necked
VR227-6	6.5	109.5	Necked
VR227-6	8.0	105.5	Necked
VR227-6	9.0	63.0	Necked
VR227-6	9.0	115.5	Necked
ZR588-6T	−13.0	46.0	Unaffected
ZR588-3	− 4.0	39.0	Unaffected
ZR588-6T	− 2.0	41.5	Unaffected
ZR566-3	− 1.0	49.5	Unaffected
ZR588-3	− 0.5	44.5	Unaffected
ZR566-3	2.0	46.0	Unaffected
ZR566-3	4.0	52.5	Unaffected
ZR566-3	4.5	54.0	Unaffected
VR227-6	8.5	57.5	Unaffected
VR227-6	9.0	60.0	Unaffected

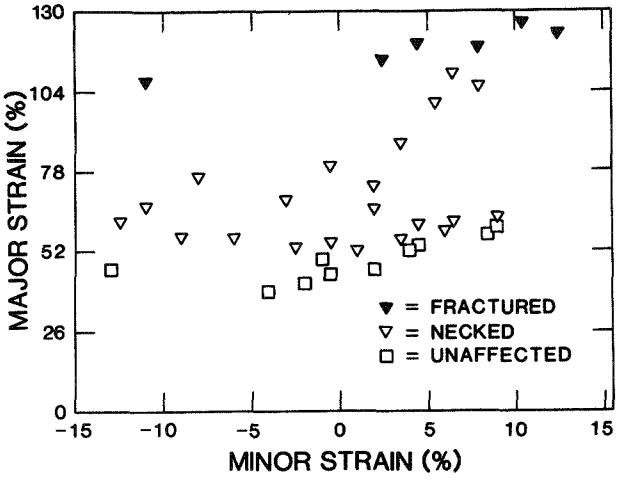

Fig. B-3. Failure limit diagram for Z-batch old-process specimens with a nominal grain size of 25 g/t, tested at 1440°C.

Table B-IV. Data Points Presented in Fig. B-4 (New-Process/B-Batch Specimens, Nominal 25 g/t, Tested at 1440°C)

Sample	Minor Strain (%)	Major Strain (%)	Condition
B1-2-6	−6.0	120.5	Fractured
B1-2-6	−3.0	126.5	Fractured
B1-2-6	−2.0	122.5	Fractured
B1-2-6	−0.5	114.0	Fractured
B1-1-5	1.5	115.0	Fractured
B1-2-6	3.5	114.5	Fractured
B1-1-5	−6.0	105.5	Necked
B1-2-6	−4.5	74.5	Necked
B1-2-6	−4.0	85.0	Necked
B1-2-6	−3.0	80.5	Necked
B1-2-6	−3.0	104.5	Necked
B1-2-6	−2.5	74.0	Necked
B1-1-5	−2.5	96.5	Necked
B1-1-5	−1.0	96.5	Necked
B1-2-6	−0.5	80.0	Necked
B1-1-5	0.0	107.5	Necked
B1-1-5	0.5	82.5	Necked
B1-1-5	1.0	---	---

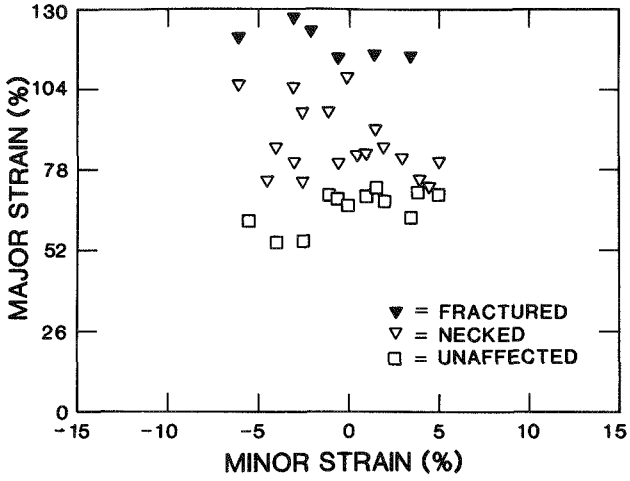

Fig. B-4. Failure limit diagram for B-batch new-process specimens with a nominal grain size of 25 g/t, tested at 1440°C.

Table B-V. Data Points Presented in Fig. B-5 (Old-Process B-Batch Specimens, Nominal 25 g/t, Tested at 1440°C)

Sample	Minor Strain (%)	Major Strain (%)	Condition
B701-1	−5.5	99.0	Fractured
B701-1	−2.0	122.5	Fractured
B701-2	0.0	100.5	Fractured
B701-2	0.5	114.0	Fractured
B701-2	1.5	119.0	Fractured
B701-2	2.5	118.5	Fractured
B701-2	6.5	115.5	Fractured
B701-2	−10.0	98.0	Necked
B701-1	−2.0	71.0	Necked
B701-2	−0.5	84.0	Necked
B701-2	0.0	87.5	Necked
B701-2	1.0	77.5	Necked
B701-2	1.0	101.5	Necked
B701-2	1.5	73.0	Necked
B701-2	2.0	103.5	Necked
B701-1	2.5	74.5	Necked
B701-2	3.0	103.0	Necked
B701-2	3.0	84.0	Necked
B701-1	4.5	66.5	Necked
B701-1	5.0	103.0	Necked
B701-2	7.0	71.0	Necked
B701-1	−2.5	59.0	Unaffected
B701-1	−1.5	66.5	Unaffected
B701-1	−1.5	59.5	Unaffected
B701-2	−1.0	51.5	Unaffected
B701-1	−0.5	66.0	Unaffected
B701-1	0.0	63.5	Unaffected
B701-2	0.5	59.0	Unaffected
B701-2	1.0	61.5	Unaffected
B701-2	2.0	62.5	Unaffected
B701-1	3.0	66.0	Unaffected
B701-1	3.5	61.0	Unaffected
B701-2	6.0	64.5	Unaffected

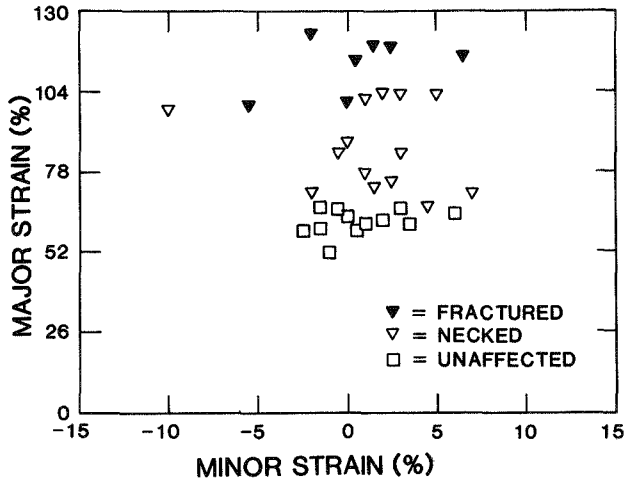

Fig. B-5. Failure limit diagram for old-process B-batch specimens with a nominal grain size of 25 g/t, tested at 1440°C.

Table B-VI. Data Points Presented in Fig. B-6 (New-Process B-Batch Specimens, Nominal 15 g/t, Tested at 1100°C)

Sample	Minor Strain (%)	Major Strain (%)	Condition
B2-8-5	−0.5	49.0	Fractured
B2-2-3	0.0	44.0	Fractured
B2-8-5	0.5	43.0	Fractured
B2-2-3	1.0	45.0	Fractured
B2-8-5	1.5	52.5	Fractured
B2-2-3	4.0	49.0	Fractured
B2-8-5	−2.0	36.5	Unaffected
B2-2-3	−1.5	34.0	Unaffected
B2-2-3	−1.0	36.5	Unaffected
B2-2-3	−0.5	36.5	Unaffected
B2-2-3	1.0	36.5	Unaffected
B2-8-5	1.5	36.5	Unaffected
B2-2-3	2.0	45.0	Unaffected
B2-8-5	3.5	41.0	Unaffected

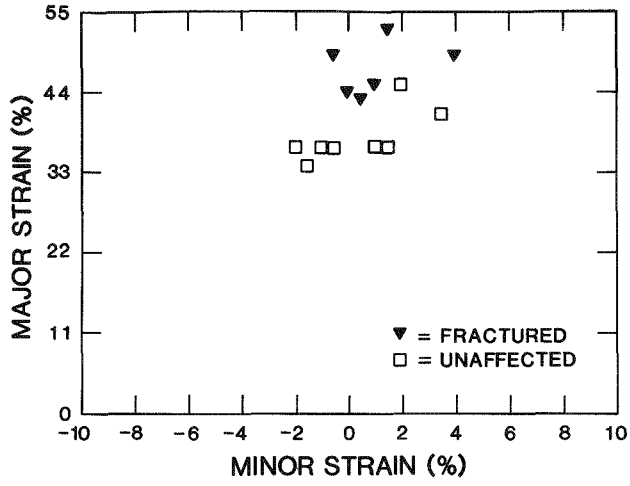

Fig. B-6. Failure limit diagram for B-batch new-process specimens with a nominal grain size of 15 g/t, tested at 1100°C.

Table B-VII. Data Points Presented in Fig. B-7 (Old-Process B-Batch Specimens, Nominal 15 g/t, Tested at 1100°C)

Sample	Minor Strain (%)	Major Strain (%)	Condition
B727-4	1.0	45.0	Fractured
B727-4	2.0	43.5	Fractured
B727-4	−1.0	35.0	Unaffected
B727-4	−0.5	37.0	Unaffected
B701-3	0.0	33.5	Unaffected
B701-3	1.5	34.5	Unaffected
B727-4	2.0	42.0	Unaffected
B727-4	2.5	36.0	Unaffected
B727-4	3.0	38.5	Unaffected
B701-3	3.5	39.5	Unaffected
B727-4	4.0	42.9	Unaffected
B727-4	4.5	44.5	Unaffected
B727-4	6.0	46.0	Unaffected
B727-4	7.5	42.0	Unaffected

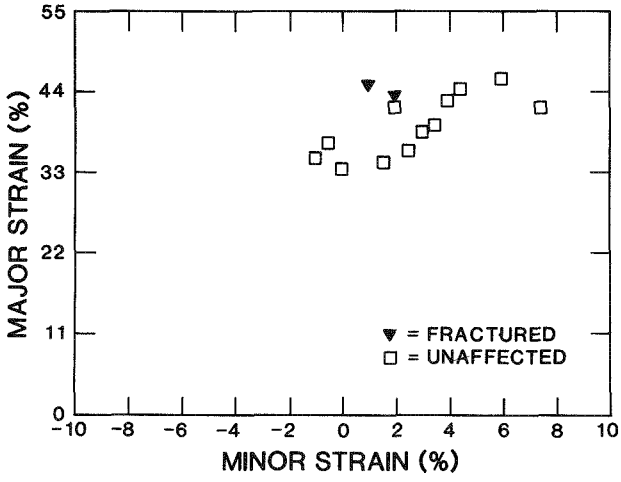

Fig. B-7. Failure limit diagram for old-process B-batch specimens with a nominal grain size of 15 g/t, tested at 1100°C.

Table B-VIII. Data Points Presented in Fig. B-8 (Z-Batch Specimens, Nominal 15 g/t, Tested at 1000°C)

Sample	Minor Strain (%)	Major Strain (%)	Condition
RR932-2	−4.0	28.5	Fractured
RR932-6	−3.5	31.0	Fractured
RR932-2	−3.0	35.5	Fractured
RR932-2	−2.5	32.5	Fractured
RR932-6	1.0	30.5	Fractured
RR932-6	2.0	32.0	Fractured
RR932-6	3.5	30.5	Fractured
RR932-6	−3.0	20.0	Unaffected
RR932-2	−2.5	17.5	Unaffected
RR932-2	−2.0	17.0	Unaffected
RR932-6	−1.0	22.0	Unaffected
RR932-6	0.0	25.0	Unaffected
RR932-6	0.5	23.0	Unaffected
RR932-6	1.0	26.0	Unaffected
RR932-6	1.5	25.0	Unaffected

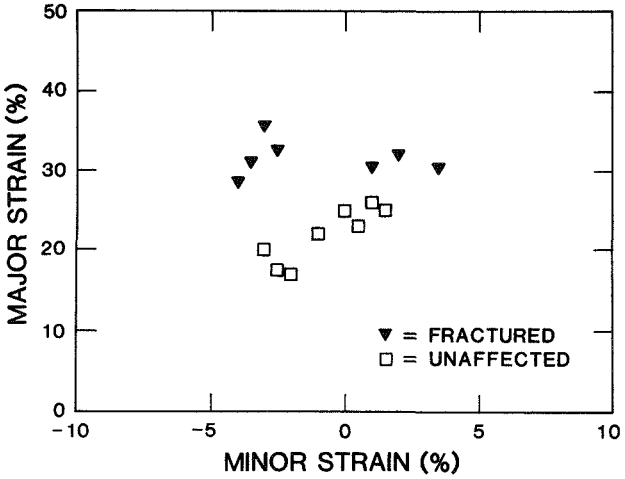

Fig. B-8. Failure limit diagram for Z-batch old-process specimens with a nominal grain size of 15 g/t, tested at 1000°C.

Table B-IX. Data Points Presented in Fig. B-9 (New-Process B-Batch Specimens, Nominal 15 g/t, Tested at 1000°C)

Sample	Minor Strain (%)	Major Strain (%)	Condition
B1-7-5	−1.5	40.0	Fractured
B1-7-5	−1.0	34.0	Fractured
B1-4-2	−0.5	34.0	Fractured
B1-4-2	1.5	38.0	Fractured
B1-7-5	3.0	35.5	Fractured
B1-4-2	4.0	45.0	Fractured
B1-7-5	−3.0	20.0	Unaffected
B1-4-2	−1.0	24.5	Unaffected
B1-4-2	−0.5	25.5	Unaffected
B1-4-2	2.0	26.5	Unaffected
B1-7-5	2.5	24.5	Unaffected
B1-4-2	5.5	26.0	Unaffected

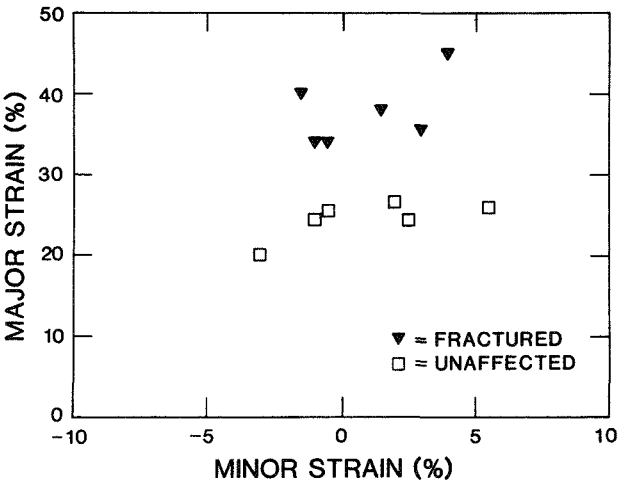

Fig. B-9. Failure limit diagram for B-batch new-process specimens with a nominal grain size of 15 g/t, tested at 1000°C.

Table B-X. Data Points Presented in Fig. B-10 (Old-Process B-Batch Specimens, Nominal 15 g/t, Tested at 1000°C)

Sample	Minor Strain (%)	Major Strain (%)	Condition
B704-3	0.0	34.0	Fractured
B704-4	0.5	36.0	Fractured
B704-4	1.0	33.0	Fractured
B704-4	2.0	38.5	Fractured
B704-3	3.0	35.0	Fractured
B704-4	3.5	35.0	Fractured
B704-3	−3.0	32.0	Unaffected
B704-4	0.5	27.0	Unaffected
B704-3	1.5	26.5	Unaffected
B704-3	2.5	30.0	Unaffected
B704-4	3.5	26.0	Unaffected
B704-4	5.0	25.5	Unaffected
B704-3	6.0	33.5	Unaffected

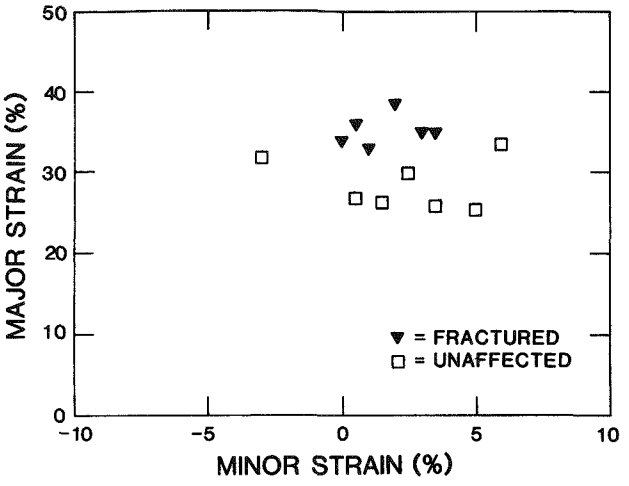

Fig. B-10. Failure limit diagram for old-process B-batch specimens with a nominal grain size of 15 g/t, tested at 1000°C.

Table B-XI. Data Points Presented in Fig. B-11 (Z-Batch Specimens, Nominal 25 g/t, Tested at 1000°C)

Sample	Minor Strain (%)	Major Strain (%)	Condition
ZR579R-5	−2.0	42.5	Fractured
ZR579R-5	4.0	44.5	Fractured
Z563-5	4.5	51.0	Fractured
Z563-5	−2.5	39.0	Unaffected
ZR576-5	−1.0	26.5	Unaffected
Z563-5	0.0	41.5	Unaffected
Z563-5	0.5	40.5	Unaffected
Z563-5	2.5	43.0	Unaffected
Z563-5	3.0	43.5	Unaffected
Z563-5	3.5	43.5	Unaffected
Z563-5	5.0	53.5	Unaffected
Z563-5	8.5	50.5	Unaffected

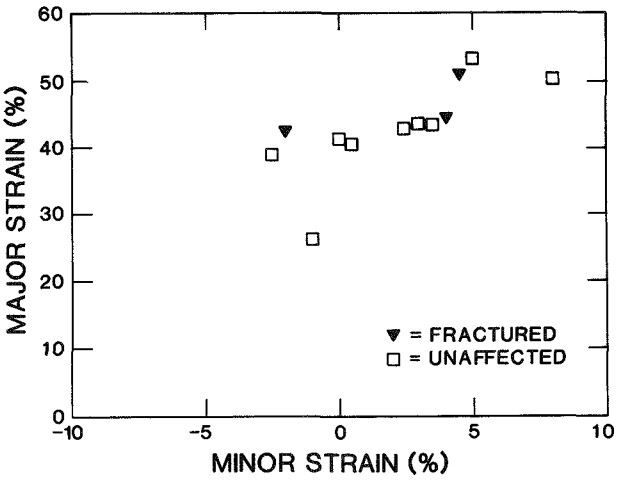

Fig. B-11. Failure limit diagram for Z-batch old-process specimens with a nominal grain size of 25 g/t, tested at 1000°C.

Table B-XII. Data Points Presented in Fig. B-12 (New-Process B-Batch Specimens, Nominal 25 g/t, Tested at 1000°C)

Sample	Minor Strain (%)	Major Strain (%)	Condition
B1-7-3	0.0	54.0	Fractured
B1-7-3	1.0	57.5	Fractured
B1-7-3	1.5	42.5	Fractured
B1-7-3	4.0	40.5	Fractured
B1-7-3	−5.0	34.0	Unaffected
B1-7-3	−3.0	33.5	Unaffected
B1-7-3	−2.0	36.0	Unaffected
B1-7-3	−1.5	37.5	Unaffected
B1-2-2	−1.0	29.0	Unaffected
B1-7-3	1.0	31.0	Unaffected
B1-2-2	1.5	31.0	Unaffected
B1-7-3	2.0	32.5	Unaffected
B1-1-1	2.5	30.5	Unaffected
B1-1-1	3.5	35.0	Unaffected
B1-1-1	4.5	36.5	Unaffected
B1-1-1	5.0	42.0	Unaffected
B1-1-1	6.0	40.5	Unaffected

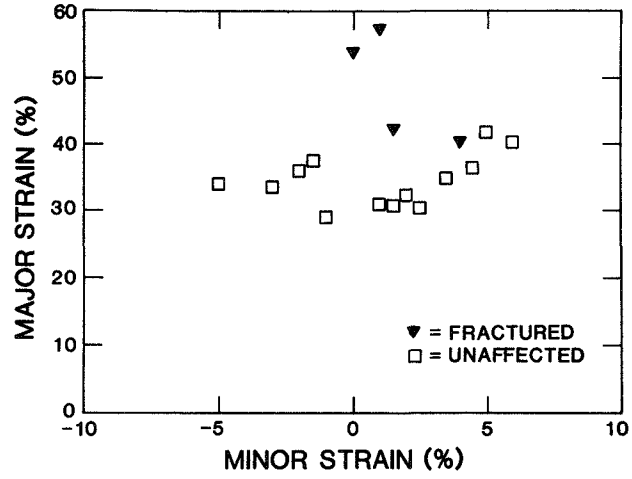

Fig. B-12. Failure limit diagram for B-batch new-process specimens with a nominal grain size of 25 g/t, tested at 1000°C.

Table B-XIII. Data Points Presented in Fig. B-13 (Old-Process B-Batch Specimens, Nominal 25 g/t, Tested at 1000°C)

Sample	Minor Strain (%)	Major Strain (%)	Condition
B703-3	−2.0	56.5	Fractured
B703-3	−1.5	55.5	Fractured
B703-3	−4.5	40.5	Unaffected
B704-1	−2.0	36.0	Unaffected
B704-1	−1.0	33.0	Unaffected
B704-1	−0.5	35.5	Unaffected
B703-3	0.5	42.5	Unaffected
B703-3	1.0	46.5	Unaffected
B703-3	1.5	42.5	Unaffected
B704-1	2.0	39.5	Unaffected
B703-3	4.0	41.0	Unaffected

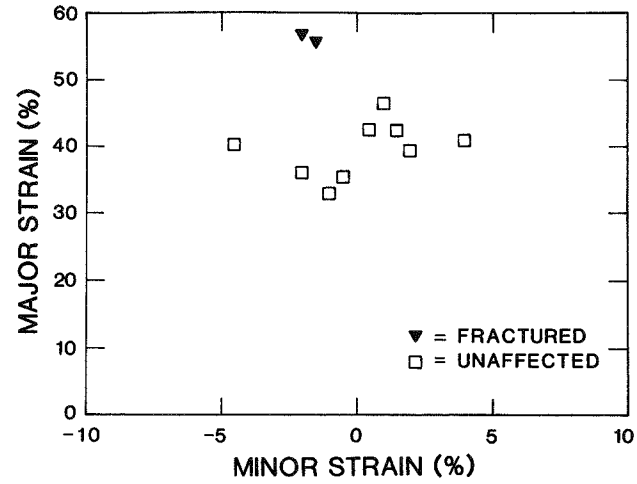

Fig. B-13. Failure limit diagram for B-batch old-process specimens with a nominal grain size of 25 g/t, tested at 1000°C.

Table B-XIV. Data Points Presented in Fig. B-14 (New-Process B-Batch Specimens, Nominal 15 g/t, Tested at 900°C)

Sample	Minor Strain (%)	Major Strain (%)	Condition
B2-1-2	−1.5	24.0	Fractured
B2-8-3	0.5	24.0	Fractured
B2-8-3	1.0	28.0	Fractured
B2-1-2	1.5	28.5	Fractured
B2-1-2	2.0	25.5	Fractured
B2-1-2	3.0	25.5	Fractured
B2-1-2	−3.0	17.0	Unaffected
B2-8-3	−2.0	17.5	Unaffected
B2-8-3	−0.5	16.0	Unaffected
B2-8-3	0.0	21.5	Unaffected
B2-8-3	0.5	22.5	Unaffected
B2-1-2	1.0	18.0	Unaffected
B2-8-3	2.5	17.5	Unaffected
B2-8-3	4.0	18.5	Unaffected

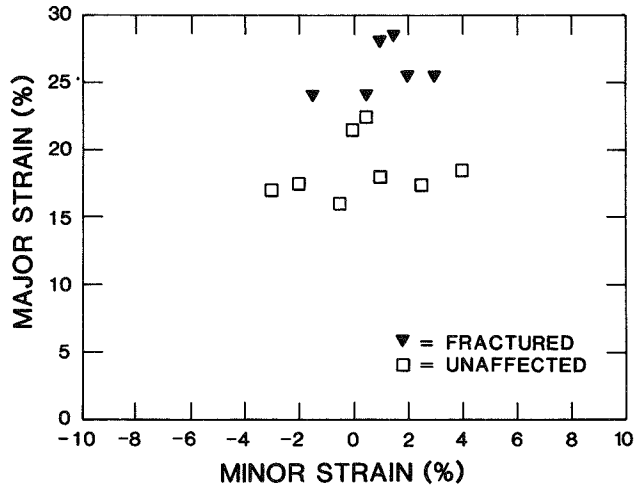

Fig. B-14. Failure limit diagram for B-batch new-process specimens with a nominal grain size of 15 g/t, tested at 900°C.

Table B-XV. Data Points Presented in Fig. B-15 (Old-Process B-Batch Specimens, Nominal 15 g/t, Tested at 900°C)

Sample	Minor Strain (%)	Major Strain (%)	Condition
B703-2	3.0	23.5	Fractured
B732-5	4.0	27.5	Fractured
B732-5	6.5	28.5	Fractured
B703-2	−1.5	15.0	Unaffected
B732-5	−1.0	17.0	Unaffected
B732-5	−0.5	22.0	Unaffected
B703-2	0.0	20.0	Unaffected
B732-5	1.0	18.0	Unaffected
B703-2	1.5	15.5	Unaffected
B732-5	2.0	20.5	Unaffected
B703-2	2.5	21.5	Unaffected
B732-5	3.5	21.0	Unaffected
B732-5	4.0	21.5	Unaffected

Table B-XVI. Data Points Presented In Fig. B-16 (New-Process B-Batch Specimens, Nominal 15 g/t, Tested at 800°C)

Sample	Minor Strain (%)	Major Strain (%)	Condition
B2-5-1	1.5	16.0	Fractured
B2-5-1	4.0	17.5	Fractured
B2-5-1	0.0	13.0	Unaffected
B2-5-1	1.5	15.0	Unaffected
B2-5-1	2.0	13.5	Unaffected
B2-2-4	2.5	10.5	Unaffected
B2-5-1	4.5	12.0	Unaffected

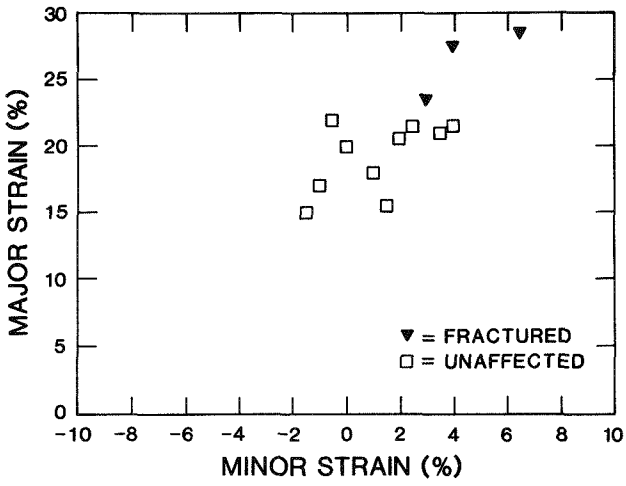

Fig. B-15. Failure limit diagram for B-batch old-process specimens with a nominal grain size of 15 g/t, tested at 900°C.

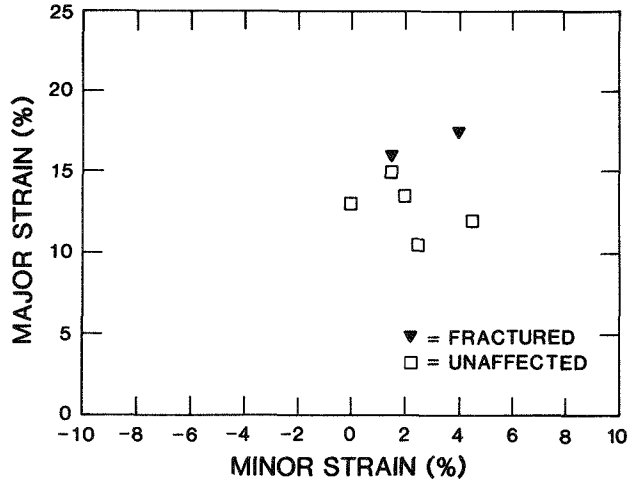

Fig. B-16. Failure limit diagram for B-batch new-process specimens with a nominal grain size of 15 g/t, tested at 800°C.

Table B-XVII. Data Points Presented in Fig. B-17 (Old-Process B-Batch Specimens, Nominal 15 g/t, Tested at 800°C)

Sample	Minor Strain (%)	Major Strain (%)	Condition
B729-2	−0.5	16.5	Fractured
B729-2	1.0	16.5	Fractured
B729-2	2.0	16.0	Fractured
B729-2	3.5	17.0	Fractured
B729-2	−2.5	13.5	Unaffected
B731-1	−1.0	15.0	Unaffected
B729-2	0.0	17.0	Unaffected
B729-2	0.5	15.0	Unaffected
B729-2	1.0	15.0	Unaffected
B729-2	1.5	15.5	Unaffected
B729-2	2.0	14.5	Unaffected
B729-2	3.0	16.0	Unaffected
B729-2	5.0	16.0	Unaffected

Table B-XVIII. Data Points Presented in Fig. B-18 (Z-Batch Specimens, Nominal 25 g/t, Tested at 800°C)

Sample	Minor Strain (%)	Major Strain (%)	Condition
Z561-6	−4.0	35.5	Fractured
Z561-6	−2.5	34.0	Fractured
Z561-6	−2.0	31.5	Fractured
Z561-6	−1.5	30.0	Fractured
Z561-6	0.0	32.0	Fractured
ZR567-5	0.5	21.5	Fractured
Z561-6	2.0	34.0	Fractured
Z561-6	−4.0	18.5	Unaffected
Z561-6	−3.0	22.0	Unaffected
Z561-6	−1.0	17.0	Unaffected
ZR567-5	0.5	19.0	Unaffected
Z561-6	1.5	16.5	Unaffected
Z561-6	2.0	17.5	Unaffected
ZR567-5	2.5	16.0	Unaffected
Z561-6	2.5	18.5	Unaffected
Z561-6	3.0	21.0	Unaffected
ZR567-5	4.0	18.5	Unaffected
Z561-6	6.5	22.0	Unaffected

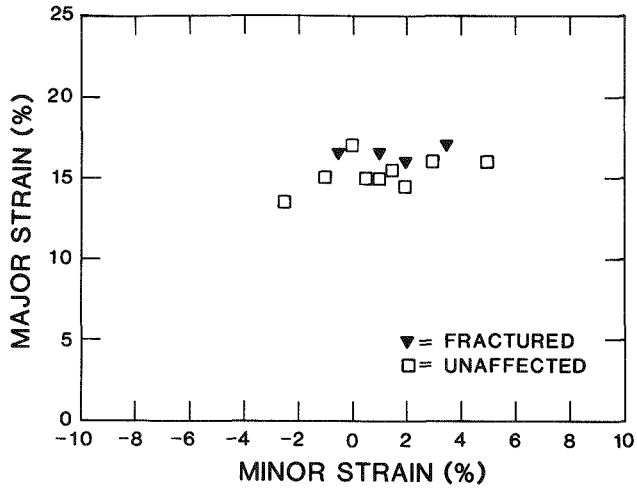

Fig. B-17. Failure limit diagram for B-batch old-process specimens with a nominal grain size of 15 g/t, tested at 800°C

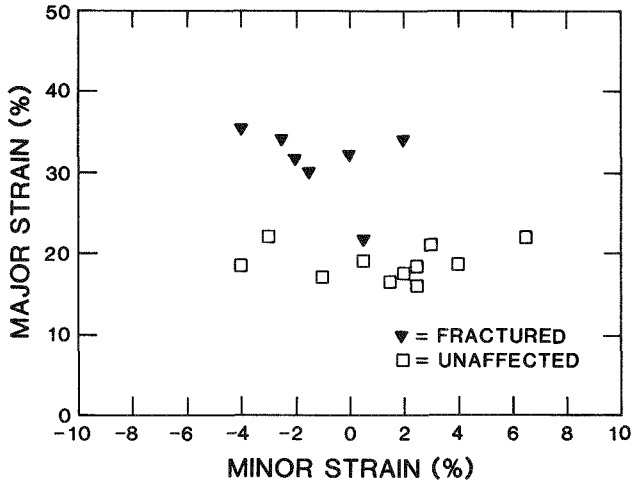

Fig. B-18. Failure limit diagram for Z-batch old-process specimens with a nominal grain size of 25 g/t, tested at 800°C

Table B-XIX. Data Points Presented in Fig. B-19 (Z-Batch Specimens, Nominal 25 g/t, Tested at 600°C)

Sample	Minor Strain (%)	Major Strain (%)	Condition
ZR563-2	−1.0	6.5	Unaffected
ZR563-2	−0.5	6.0	Unaffected
ZR563-2	0.5	6.0	Unaffected
ZR563-2	0.5	7.5	Unaffected
ZR563-2	1.0	7.5	Unaffected
ZR563-2	2.5	9.5	Unaffected
ZR563-2	2.5	13.0	Unaffected
ZR563-2	4.0	13.0	Unaffected
ZR563-2	7.0	13.5	Unaffected

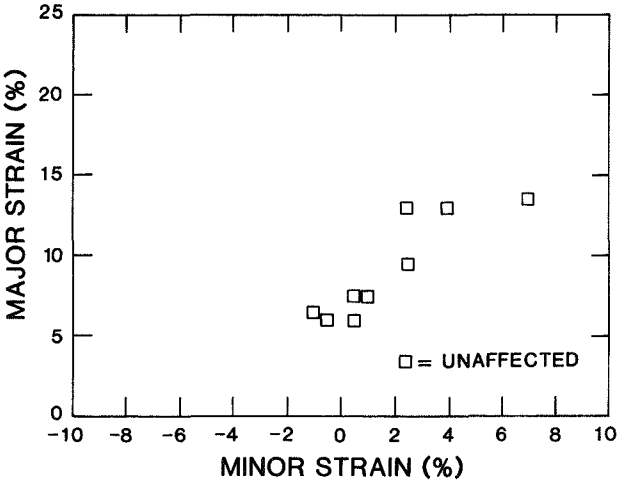

Fig. B-19. Failure limit diagram for Z-batch old-process specimens with a nominal grain size of 25 g/t, tested at 600°C